

Dareplane: A modular open-source software platform for BCI research with application in closed-loop deep brain stimulation

Matthias Dold^{1,2,3}, Joana Pereira^{3,1,4}, Bastian Sajonz³, Volker A. Coenen³, Jordy Thielen¹, Marcus L.F. Janssen², Michael Tangermann¹

¹ Data-Driven Neurotechnology Lab, Donders Institute for Brain, Cognition and Behaviour, Radboud University, The Netherlands

² Department of Clinical Neurophysiology, Maastricht University Medical Center, The Netherlands; Mental Health and Neuroscience Research Institute, Maastricht University, The Netherlands

³ Department of Stereotactic and Functional Neurosurgery, Medical Center – University of Freiburg, Faculty of Medicine, University of Freiburg, Germany

⁴ BrainLinks–BrainTools Center, University of Freiburg, Germany

E-mail: matthias.dold@donders.ru.nl

Abstract.

This work introduces Dareplane, a modular and broad technology-agnostic open source software platform for brain-computer interface research with an application focus on adaptive deep brain stimulation (aDBS). While the search for suitable biomarkers to inform aDBS has provided rich results over the last two decades, development of control strategies is not progressing at the same pace. One difficulty for investigating control approaches resides with the complex setups required for aDBS experiments. The Dareplane platform supports aDBS setups, and more generally brain computer interfaces, by providing a modular, technology-agnostic, and easy-to-implement software platform to make experimental setups more resilient and replicable. The key features of the platform are presented and the composition of modules into a full experimental setup is discussed in the context of a Python-based orchestration module. The performance of a typical experimental setup on Dareplane for aDBS is evaluated in three benchtop experiments, covering (a) an easy-to-replicate setup using an Arduino microcontroller, (b) a setup with hardware of an implantable pulse generator, and (c) a setup using an established and CE certified external neurostimulator. Benchmark results are presented for individual processing steps and full closed-loop processing. The results show that the microcontroller setup in (a) provides timing comparable to the realistic setups in (b) and (c). The full technical feasibility of the platform in the aDBS context is demonstrated in a first closed-loop session with externalized leads on a patient with Parkinson's disease receiving DBS treatment and further evaluated in a non-invasive BCI speller application.

Keywords: Deep brain stimulation, closed-loop, open source software, brain-computer interface, electrophysiology, brain-machine interface

Submitted to: *J. Neural Eng.*

1. Introduction

A brain computer interface (BCI) is defined by the BCI Society [1] as a system that measures brain activity and derives outputs to interact with its environment. This definition also comprises invasive closed-loop systems which are often referred to as brain machine interfaces (BMI) [2]. To realize a BCI, various processing steps and inherent challenges need to be considered: (1) Data is acquired from potentially multimodal sources. Especially for non-invasive signals, this might result in low signal-to-noise (SNR) levels. (2) The neural activity is decoded with algorithmic approaches that can have high complexity. (3) Feedback and control strategies are applied to the decoded signal. These strategies often need to be able to cope with non-stationarities in the decoded data distributions. (4) Feedback is then provided based on the controller output via hardware interfaces. A potential processing step (5) is the provision of a behavioral paradigm which needs to be accurately synchronized to the data acquisition. The challenges in the sequence of these five processing steps become even more pronounced when patient experiments are considered, which usually adds scarcity of data acquisition opportunity to the constraints. In the context of deep brain stimulation (DBS) research, and specifically adaptive DBS (aDBS), which motivated this work, domain-specific requirements include safety considerations for the feedback/stimulation, and performance considerations for feedback latencies.

As a consequence, researchers are investing significant time into the development of software tools to run such individual experiments - while on an abstract level, there is a substantial streamlining potential for BCI experiments along the processing steps (1) - (5).

The proposed data-driven research and evaluation platform for neurotechnology (Dareplane) aims to facilitate this streamlining potential by providing a free and open-source software modular solution which allows the implementation and reuse of modules for BCI applications, including aDBS research.

DBS is typically delivered via a pair of DBS leads each with multiple contacts. When fully implanted, the leads are connected to an implantable pulse generator (IPG) which delivers short electric pulses to the target region, by voltage or current control between individual contacts (bipolar stimulation) or between contacts and the casing of the IPG (monopolar stimulation). Individual pulses are defined by parameters like amplitude, pulse width or shape, and are repeated with a certain stimulation frequency [3].

DBS modulates neural activity to alleviate symptoms of various neurological conditions, including Parkinson's disease (PD), essential tremor (ET), or dystonia [4]. More recently, DBS has also been proposed as a treatment for psychiatric disorders [5, 6] such as obsessive-compulsive disorder [7, 8], major depressive disorder [9–12], and Tourette syndrome [13]. Given this wide range of applications, it is not surprising that research on DBS is an increasingly active field [14], with multi-center studies and larger participant counts becoming more common in recent publications [15]. It is important to note that the exact mechanism of action of DBS is still not fully understood, and thus also subject to current research [4, 16–20] putting emphasis on the need for software platforms supporting this work.

One particular question of interest is whether the therapeutic DBS application, which is applied 24/7 and with fixed stimulation parameters, can be improved by using

closed-loop strategies, realizing aDBS. Such a closed-loop strategy would read out brain activity from the patient and could adjust the stimulation parameters according to a control strategy. In the context of PD, the search for an aDBS strategy became an increasingly popular research topic [21], after the work of Little et al. [22], which showed that aDBS achieves superior therapeutic efficacy with only 50% of the delivered charge of continuous DBS (cDBS). Various other aDBS systems have since been implemented for PD, modulating stimulation amplitude, frequency or pulse width delivered by the IPG [23–26].

Given the more than 10 years of history since the publication of Little et al. [22], it is interesting to note that the research in the applied control strategies is not developing in the same pace as the search for markers. Control strategies based on thresholds [22–24, 27, 28] are the most dominant approach. The few exceptions proposed reinforcement learning [29], proportional(-integral) control [26, 30], or threshold strategies based on time-integrated measures [31].

Taking the engineering perspective on aDBS, there are a variety of challenges, which in part apply to other BCI applications as well. First, data acquisition is limited by the accessibility of IPGs [3] with sensing capability for therapeutic aDBS, or the availability of experiments with externalization [32, 33] in the research context exclusively. The recorded data can have a low SNR and is further polluted by physiological and stimulation artifacts [34, 35]. Decoding the brain state requires considering non-stationarities on multiple time scales [36] and further adapting the stimulation to the patients motor state [28, 37]. On the feedback end, the broad range of stimulation parameters, results in a large search space that

leads to a challenging optimization problem.

The scheme in Figure 1 shows how the generic processing steps (1) - (5) mentioned above are connected in an aDBS setup, putting emphasis on the inherent modular structure. E.g., streaming data from signal recording hardware would be a data input/output (I/O) type module. Data preprocessing and decoding, potentially solving a machine learning problem [38, 39], are steps of a decoding type module. In the aDBS context, such a decoded signal can be referred to as a biomarker [16, 40] if it is also informative about the symptomatology of the disease treated with DBS. Based on the biomarker, a control strategy is then applied to derive a suitable stimulus output in what would be a control module. Such a control module would also contain safeguard mechanisms to enforce constraints on the outputs, which would trigger stimulation, or more generally feedback, via what would be a stimulation I/O type module. Finally, a behavioral paradigm such as the CopyDraw task [41] would be run within a paradigm type module. If the code base for such a setup is modular, changing e.g. the recording hardware is as easy as replacing the data I/O module, thus keeping the remaining well-tested modules.

Modularity also provides advantages purely from a systems design perspective [42, 43] and has an extended history in the context of software development for the processing of electrophysiological signals [44]. For many years, modularity has been considered as the key to code reusability [45] and is encouraged as a decision to be made early in the design process [46]. It keeps complexity manageable and inherently allows for parallelism in work [43]. Modularity also leads to well isolated errors which are faster to fix and facilitates parallel development with multiple developers. In the

academic context, it makes projects more accessible, allowing, e.g., student projects on the limited scope of individual modules.

Looking at the alignment of processing steps in Figure 1 it becomes clear that many are generic and could be reused in any open-loop or closed-loop BCI experiment and not just exclusively in aDBS. While, e.g., recording electroencephalography (EEG) signals is a highly generic task, the actual implementation might be equally specific and highly constrained with a vendor’s API only being available from a specific programming language or operating system. A software platform therefore needs to support multiple different hardware interfaces, if reuseability is desired. As a consequence, the platform should be broadly technology agnostic.

Finally, aDBS researchers who are not working on a single vendor system exclusively, will use a substantial amount of bespoke software components. To be useful for this group, and to a large user base in general, any new platform should provide a high level of ease-of-implementation for adopting existing components, minimizing the overhead needed for the integration.

Overall, we identify three structural requirements for an aDBS platform: 1) being modular for reusability and robustness, 2) being technology agnostic to integrate with different hardware and 3) providing ease-of-implementation for integration of existing code/software.

At the point of writing, we are not aware of any existing software platform dedicated to aDBS research. But, as many technical challenges are shared with general BCI applications, would any existing BCI platform meet the requirements for aDBS research? Reflecting on a few well-established BCI platforms and some more recent additions to the

platform landscape, we consider the platforms compiled in Table 1. On a high level, we can categorize the platforms in (a) large scope platforms which partially bring their dedicated hardware - the “batteries included” package [47, 48], (b) platforms which allow users to define computations as graphs [49–52] with the aim of reducing development complexity, and (c) platforms which predominantly focus on a single programming language [53–57], requiring implementations of closed-loop setups to follow their coding conventions. The three platform categories address some of the three requirements (modularity, technology agnostic, and ease of implementation) in different ways. The “batteries included” platforms cover many hardware interfaces out of the box, but come with a large core package lacking the ease of implementation for existing code and providing a limited level of modularity. Platforms with graph-based computations are inherently modular in the computation nodes, but require implementations with extended constraints to allow the integration of such nodes. In addition, this technology is typically limited to the main language of the platform (i.e., not technology agnostic). The single programming language segment by definition is not technology agnostic and neither is modularity ensured, but it can be realized depending on the actual implementation details.

Reflecting back on the processing steps (1) - (5) that need to be fulfilled for an aDBS platform none of the existing frameworks, except for BCI2000 [47], would provide control of DBS stimulation hardware out of the box. Although open-source software can always be extended, the development effort to add control functionality for stimulation varies strongly between platforms, depending on the imposed constraints and the availability of APIs for the stimulation hardware. As the

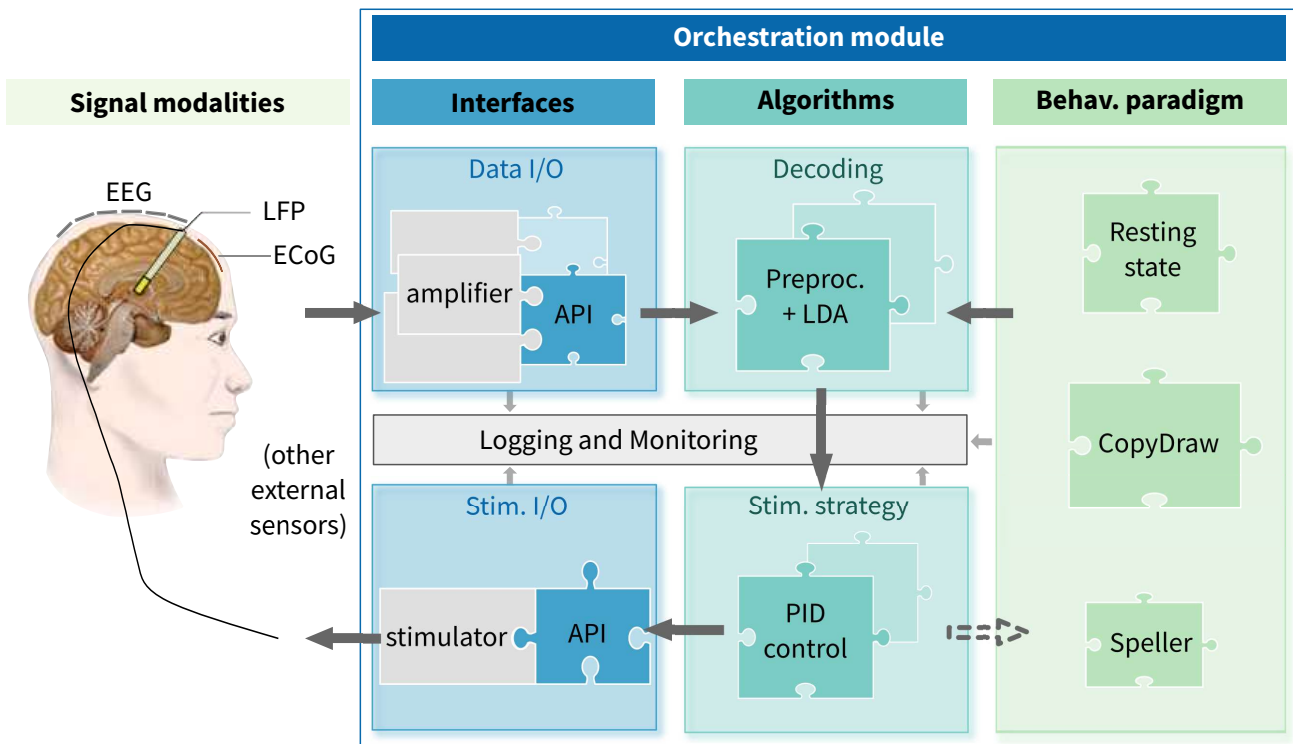


Figure 1: An abstract view of aDBS processing steps. The components can be segmented into three types: 1) I/O for interaction with hardware, either for collecting data or setting stimulation commands (providing feedback for BCIs). 2) Algorithmic components which relate to the decoding of information from the recorded signals and/or evaluate a control strategy based on a biomarker which is extracted from the signal. Such a controller could trigger stimulation in an aDBS setting, or could e.g. select a symbol in a c-VEP speller (see methods section). 3) Presentation of a behavioral paradigm in e.g. displaying a speller matrix or providing a trace to copy by handwriting for the CopyDraw task. Experimenters will usually have a central orchestration of these tasks, to be able to start/stop and modify from a single interaction point. In case the abstract modules - here shown as jigsaw puzzle pieces - are implemented independently, LSL can be used for data transfer between modules and allows a centralized logging and monitoring.

Name	Core Tech.	License
BCI2000 [47]	C++	GPL
Open Ephys [48]	C++	GPL3
OpenViBE [49]	C++	AGPL3
Falcon [50]	C++	GPL3
BRAND [51]	C++/python	MIT
Timeflux [52]	python	MIT
BCIPy [53]	python	Hippocr.
BBCI [54]	MATLAB	MIT
PyFF [55]	python	GPL2
FieldTrip [56]	MATLAB	GPL
MedusaBCI [57]	python	CCPL

Table 1: Non-exhaustive list of BCI platforms and frameworks for running closed-loop experiments. Bold-face marks software projects that showed activity since January 2023.

three requirements (modularity, technology agnostic, and ease of implementation) are only

partially fulfilled by existing platforms, and since additional development effort for adding functionality would be necessary, we decided to develop Dareplane as a modular open-source platform to match the requirements and provide functionality tailored for aDBS research.

Like Dareplane, all of the aforementioned platforms are open-source tools. Open-source software in research offers several advantages: it has the possibility to develop features more rapidly, provides more accessible collaboration opportunities, and attracts industry partners for contributions, as evidenced by the success of Lab Streaming Layer (LSL) [58, 59] third-party applications. Having a fully open-source platform also enhances the reproducibility of

research results and aligns with open research initiatives common in many fields. For these reasons, we provide the existing Dareplane modules under the permissive MIT licence.

The remaining manuscript follows along four core questions: Q1) How can a modular, technology-agnostic, and easy-to-implement platform be realized? Q2) What latencies for BCI control can be achieved with the proposed platform on different hardware setups and are they sufficient for aDBS research? Q3) Does the novel platform enable aDBS in a patient experiment with externalized DBS leads? Q4) Is the platform also able to support a code-modulated visual evoked potential (c-VEP) BCI, which servers as an example of a timing-critical application? The questions are answered along the following structure: section 2 describes the design and capabilities of the platform, reflecting on the relevance for aDBS research, before we present in section 3 the results of performance tests on benchtop setups, results of an aDBS experiment with a patient with PD, and results from three closed-loop c-VEP sessions as a proof of technical feasibility. Finally, the platform design and the results are discussed in section 4 and concluded in section 5.

2. Methods

2.1. Realizing modularity in a technology agnostic setup

The following section describes how the Dareplane platform addresses Q1, the question of how to implement a modular, technology agnostic, and easy-to-implement platform.

Modularity for the Dareplane platform is provided by a segregation of the processing steps and the use of common interfaces. The processing steps (1) - (5), which were intro-

duced above, provide a very high level of separation into single responsibilities. Staying on this high abstraction level has the advantage of limiting the complexity of the interaction protocols of the modules. Alternatively, on the other end of the spectrum from abstract to explicit, modularity could be defined on a class/struct implementation level. This would already prescribe a certain software technology, or require wrapper code, and would require adhering to the naming conventions of attributes and methods. Cutting modules in such a way leads to constraints, which increase the complexity of the setup, but are irrelevant to the actual processing steps of aDBS. It therefore is helpful to stay abstracted from implementation details and focus on the processing steps that need to be solved, keeping the interaction protocols as unified and unconstrained as possible. To this end, each module will either consume and/or produce streaming data and will have a limited set of commands exposed for controlling it.

For sharing data, we decided to make use of the well-established LSL [58, 59] framework which allows the synchronisation of data streams across networks with reliable millisecond precision. LSL is a well-accepted standard with more than one hundred client applications, i.e., software, which is freely available and commonly used in the context of BCI research. This includes clients for many recording systems provided by the vendor companies. These clients can be readily used for the data input processing step (1) within the Dareplane platform. LSL can also be considered technology agnostic as it provides a dynamic library `liblsl`, which has bindings to most programming languages relevant in the BCI field.

To allow the synthesis of different modules into a complex systems setup, i.e., module in-

teraction, we rely on an API-like structure for each module. In particular, every module communicates via a TCP/IP socket, a basic technology available to almost any relevant programming language. Implementing a TCP/IP communication server can oftentimes be easily wrapped around existing programmes and scripts with little overhead - see the python example in Listing 1 - addressing the ease-of-implementation requirement. With these minimal requirements on the functionality of a module, Dareplane should be kept attractive for development and extension.

For the communication itself, a simple structure is used which contains a so-called primary command (PCOMM) and potentially an additional json payload. The idea lends itself from the hypertext transfer protocol [60] (http) methods such as POST or GET. In an abstracted view, the method tells the server how to process the payload which contains key-value pairs relevant for such processing. On Dareplane, every module is free to implement its own primary commands that are then linked internally to the functionality the module wants to expose. A simple 'START_REC' command would be an example for a data I/O module to start the recording process. A reasonable payload to be sent alongside this command could contain the name of a file to store to, e.g., `{"file_path": "./data/my_storage_file.xdf"}`.

Requiring modules to expose functionality via TCP communication also allows to integrate modules with other non-Dareplane tech stacks that provide TCP communication. Together with the use of LSL for data streaming, this makes the platform mainly technology-agnostic.

2.2. Designing a Dareplane module

Based on the design considerations, any software which can be run in an independent process, exposes its core functionality via the PCOMM structure, and provides and/or produces data to LSL streams, can be considered Dareplane-compliant, i.e., it can be used as a Dareplane module. A comprehensive minimal example can be found in the `hello_world` example as part of the Dareplane main repository (see section 3). Additionally, a setup script is provided at <https://github.com/thijor/dp-cvep> to download and configure the modules required to run a c-VEP matrix speller. Creating a Dareplane setup with this script provides a wholistic example application, also showcasing how the central orchestration can be used to run experiments.

As most of the current development on the Dareplane platform is done in Python, we provide an utilities library, `dareplane_utils`, which can be installed via the `pip` package manager as `pip install dareplane-utils`. Getting a custom python tool wrapped to be Dareplane compliant is then as easy as using the `DefaultServer` class from `dareplane_utils` and providing it with a dictionary of PCOMMs. The `DefaultServer` is implemented to accept a TCP connection and has a parser which will interpret incoming PCOMM messages to invoke the callable that is matched by key of the prefix. For the example provided in Listing 1, a PCOMM message of `DECODE{"n": "1"}` would lead to a function call equivalent to `run_decode(n="1")` in Python.

The implementation of such a communication layer can then be tested independently by any tool capable of creating a TCP connection and sending text messages, e.g., using `telnet`. While the TCP socket allows any binary string to be communicated, there is a lim-

itation depending on how the message is decoded. For the current python modules using the `DefaultServer` from the `dareplane-utils`, PCOMMs are decoded as ASCII and therefore need to contain valid ASCII symbols. Furthermore, the pipe symbol (`|`) is used as a delimiter between the command and the payload and must therefore not be used within either. Finally, the PCOMM is supposed to end on a semi-colon (`;`) which is therefore also a reserved symbol.

```

from dareplane_utils.default_server.
    server import DefaultServer

# Assuming there is a 'decoder.py'
# script containing the callable '
# run_decode'
from decoder import run_decode

def main(port: int = 8080, ip: str =
    "127.0.0.1"):

    # The callable 'foo' will be
    # exposed as PCOMM 'DECODE'
    pcommand_map = {"DECODE":
        run_decoder}

    server = DefaultServer(port, ip=
        ip, pcommand_map=pcommand_map,
        name="decoder_server")
    server.init_server()
    server.start_listening()

```

Listing 1: Python wrapper example to expose the function `run_decode` as a Dareplane module.

2.3. Managing modules with the Dareplane control room

The control room module (*dp-control-room*) is used to compose multiple Dareplane modules into a Dareplane setup. It orchestrates other modules which are configured in a TOML file. Having a central orchestration or master module is a well-established pattern for modular designs [42].

The *dp-control-room* manages different modules as subprocesses for which it provides the book keeping, i.e., managing the life cycle from spawning the processes, connecting via TCP/IP to the module's TCP servers (each running at its own port on the local host), and finally stopping the process and potential child processes during a shutdown. Besides the module connections, the control room provides a web graphical user interface (GUI), a logging server that consolidates logging messages into a single log file, and a callback server which allows PCOMMs to be sent across modules. A schematic overview of this functionality is provided in Figure 2.

By spawning modules as individual subprocesses, Dareplane setups are inherently asynchronous across different modules. Managing the concurrency will then be a task of the operating system kernel, which is highly optimized for this purpose. Concurrency can be increased even further by designing individual modules to perform their internal tasks concurrently, if necessary.

```

[python]
# path to the root of the modules
modules_root = "../"

# names of a module to be used (
# folder name)
[python.modules.dp-cvep-decoder]
type = "decoder"
# if no port is provided, a random
# free port is chosen
port = 8082
ip = "127.0.0.1"

```

Listing 2: Configuration example of adding a module *dp-cvep-decoder* to a Dareplane setup. The module will have its communication server available at `127.0.0.1:8082`.

2.3.1. Configuration of Dareplane setups

Modules are loaded from the *dp-control-room* according to TOML configurations, e.g., in

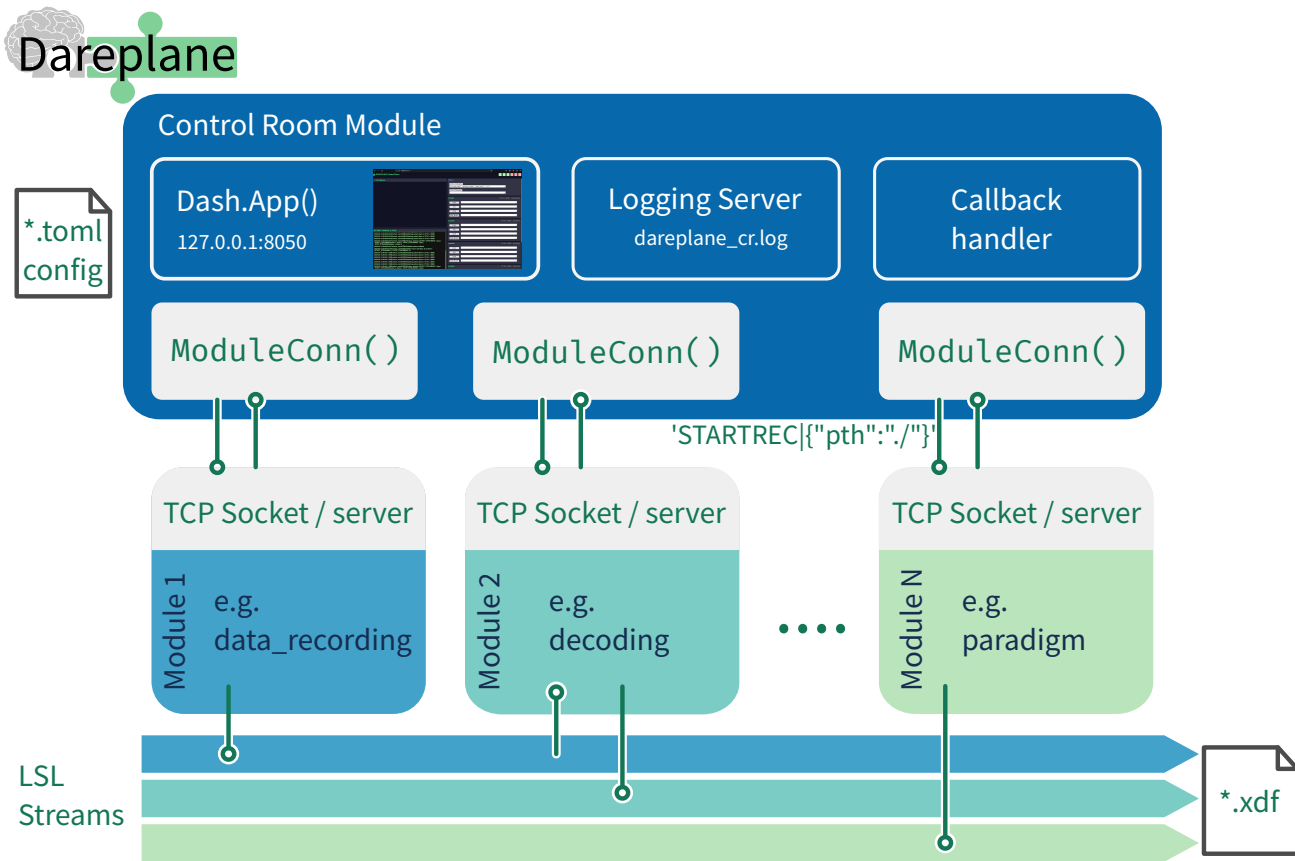


Figure 2: Control room orchestration schema. The control room module orchestrates a Dareplane setup by spawning different modules as subprocesses and connects to them via TCP sockets for sending primary commands such as e.g., `STARTREC[{"pth":"./"}]`. Individual modules communicate data via LSL streams where each module can send to or listen to one or multiple streams. Modules can also trigger a function of another module by sending a callback via TCP/IP which is processed in the control room. The user interaction is done via a web GUI which is served by the control room on the localhost. A central logging server is started at port 9020 which is the default for Python TCP logging, allowing individual modules to log to a single log file.

a `config.toml` file. An example of such a configuration is provided in Listing 2. It specifies that modules based on python will be located in the `modules_root` folder. In this folder, it would look for a module `dp-mockup-streamer` in a folder with the same name and would start the module's TCP server under `127.0.0.1:8082`.

All modules will have individual controls, i.e., buttons for their PCOMM's visible in the web GUI. In case a chain of multiple commands is to be started, `macros` can be defined inside the same `config.toml` containing the modules for loading. Each macro is defined by a unique name, a chain of commands it executes according to the

alphabetical order of the keys they are defined under, and macro parameters which can be passed to the individual processing steps. See Listing 3 for a minimal example which shows how a macro can be used to combine calling the functionality of multiple modules. In the example, three steps are executed. In the first step, the `dp-cvep-decoder` loads the model for the provided file name. The command is triggered by the `dp-control-room` sending `LOAD[{"model": "test_cvep_1.joblib"}]` to the `dp-cvep-decoder`. The payload is providing the key value pairs, here in the macros `cmd` section. While the key (left side) will be used in the payload string, the right side refers to variables defined in the `default_json`

section of the macro definition. Any key value pairs of this section will appear in the GUI, see Figure 3 (D). A template structure with `<key_name>` is used to conveniently change multiple variables. In the provided example, changing the value of `block=2` in the GUI, would result in using `fname="test_cvpep_2.joblib"` when running the macro. Changes of these key value pairs are evaluated once the macro button is pressed.

```
[macros]
[macros.start_online]
  # the name will appear on the
  # button in the web GUI
  name = "START Online"
  description = "Start an online
  run with the speller and the
  decoder"
[macros.start_online.default_json]
  block = 1
  fname = "test_cvpep_<block>.
  joblib"
[macros.start_online.cmds]
  # [<target_module>, <PCOMM>, <
  # kward_name1 (optional)>, <
  # kward_name2 (optional)>]
  com1 = ["dp-cvpep-decoder", "LOAD"
  , "model=fname"]
  com2 = ["dp-cvpep-decoder", "
  CONNECT"]
  com4 = ["dp-cvpep-speller", "
  RUN_ONLINE"]
```

Listing 3: Configuration of a macro for 'start_online'. First, the decoder module loads a model file, using the `LOAD` PCOMM with a payload of `{"model": "test_cvpep_1.joblib"}`. Next, the decoder will connect to the data stream by calling the `CONNECT` PCOMM. Finally, the `RUN_ONLINE` PCOMM of the `dp-cvpep-speller` module is called. All this can be triggered by a single button press. The button will be labelled with 'START Online'. All PCOMMs need to be implemented in the according modules (exposed from their servers). Macros are defined by the user in config TOML files.

The second step of the macro will execute the `CONNECT` command, e.g., to connect the decoder to the LSL stream of the paradigm. In this case the PCOMM would not contain a payload and would be `CONNECT|;`

. The last command of the macro would invoke the `RUN_ONLINE` again with a PCOMM without payload, i.e., `RUN_ONLINE|;`

Once configured, the `dp-control-room` creates a web application based on the Python library `dash`. It runs on the localhost at port 8050, which can be accessed via any web browser, see Figure 3 (A). Having a local web server allows to make the control room accessible to other devices, provided the local network is setup accordingly. On the webpage (GUI) the experimenter is provided with information about active LSL streams Figure 3 (B), the latest lines of the central logging file Figure 3 (C) and the status of the servers for each individual module Figure 3 (F). These views update on a 3s interval. Figure 3 (D) shows a segment which is populated with the macros specified in the config TOML. For each macro, a button for running the macro and a free text field for providing parameters in json is created. The content of the free text field is populated according to the 'default_json' values in the config TOML file - c.f. Listing 3. A validation routine will change the background of the text field if the provided text is not a valid json string. Figure 3 (E) shows the sections for each individual module, providing a button and text field for each primary command exposed by the module. These buttons are especially useful for system tests or during debugging as they allow a quick access to all of a module's exposed functionality.

2.4. Closed-Loop Communication

Using individual modules spawned up via the control room allows to easily compose complex setups. Up to this point, it was shown how functionality can be made Dareplane compliant and how modules are

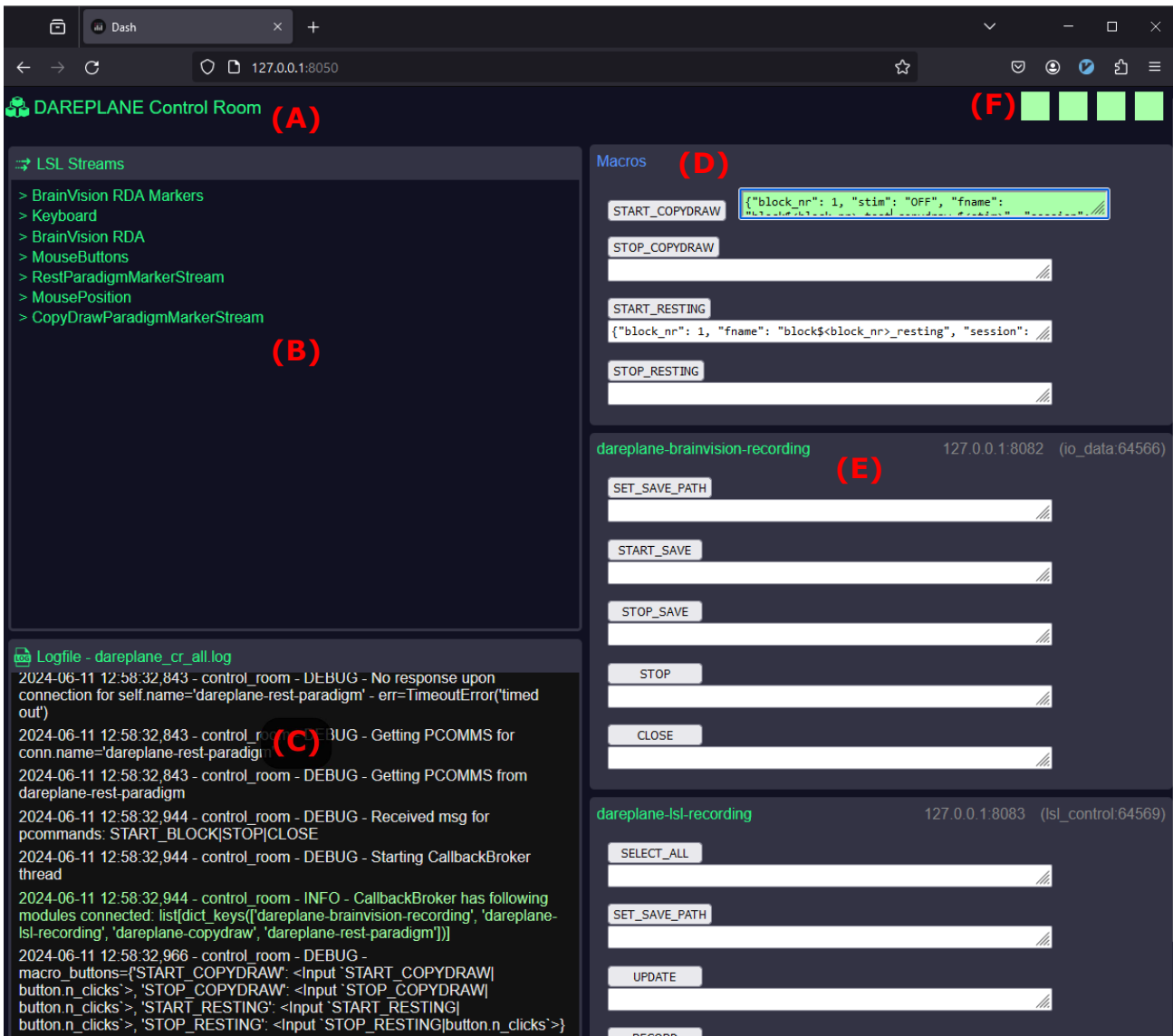


Figure 3: The web application spawned by the *dp-control-room* module. (A) Shows the application running on localhost at port 8050. It could be reached by other devices depending on the network settings. (B) A tile on the GUI lists active LSL streams. (C) The last entries in the central log file are shown in another tile. Both, (B) and (C), are updated in 3s intervals. (D) The macro section is populated with pairs of buttons for running the macro and a free text field for providing parameters in json format. The content of the free text field is pre-filled according to the ‘default_json’ values in the config TOML file. (E) A module section is spawned for each configured module, exposing all available primary commands, providing quick access testing and bug fixing. (F) Indicator blocks for each module show if the module server is responding via TCP. The control room is pinging the module servers every 3s and adjusting the color to red if no response is returned. The boxes provide details about the module servers on hover.

managed by the *dp-control-room*. The final step for a closed-loop setup is to understand how modules interact. Dareplane provides two different approaches for inter module communication:

- (1) Using an **LSL stream** which is populated by the source modules and which is subscribed to by the target module.

- (2) Using **primary command callbacks** which are triggered via the control room by TCP/IP communication.

Using an LSL stream, named, e.g., “decoding2paradigm”, would be the most canonical approach to allow the sharing of time series data or discrete markers. The target module would be implemented with a listener

(LSL inlet) on the given LSL stream and would process the stream values. In this example, the “decoding2paradigm” stream could contain a marker emitted from a decoding source module (LSL outlet), which, e.g., for a BCI speller setup would contain `selected:A` . Then the target module, e.g., the speller paradigm module could stop iterating through the speller matrix and mark the letter `A` as chosen. Analogously, a source module for closed-loop stimulation could be the control module which derived a target stimulation from decoded biomarkers using its control algorithm. The target stimulation amplitude could then be a time series that the control module would broadcast. Based on this time series, the stimulation module would select a stimulation amplitude.

The second possibility, using primary command callbacks, does not allow to share time series signals, but can trigger primary commands of any target module. It uses the existing socket connection between the individual modules and the control room. Such a primary command callback is triggered by a message adhering to the structure `<target_module>|<PCOMM>—{potential json payload};` , which is sent from any module to the control room via TCP socket connection. The first segment in the message informs the control room about which target module to send the rest of the message to via its socket connection. The message has to contain a valid PCOMM, which needs to be ensured by the implementation in the source module. This method of closing the loop is implemented in Python (since *dp-control-room* is a Python module) and is especially suited for less time critical interventions or helpful if the target module cannot implement an LSL inlet. Furthermore, it can be used if an ex-

isting module should trigger any functionality which should be separated from the module itself. E.g., a target module could create backups of a file, which is triggered by a source module that has finished recording to that file.

2.5. Benchtop Tests

The performance of running closed-loop experiments with the Dareplane platform was tested in a benchtop environment using the arbitrary waveform generator (AWG) of an oscilloscope as a signal source. These tests were conducted to answer Q2 which investigates latencies that the Dareplane platform is able to achieve with different hardware in an aDBS closed-loop.

We conducted three different benchtop tests to evaluate the performance of generic, but realistic scenarios of using of Dareplane within an aDBS experiment. As the processing requirements of a full pipeline can be highly varying, considering, e.g., sampling frequencies and inference frequency for control decisions, the performance tests were conducted with very simplistic processing requirements. Any reported processing latencies are therefore to be understood as capturing especially the overhead of network and memory I/O induced by pulling and pushing from and to different LSL streams, as well as hardware-specific overheads. All tests were run on the same Thinkpad Notebook containing an Intel i7-8750H CPU, 16 Gb of RAM and an NVIDIA Quadro P1000 GPU. All modules used for testing are available on github at <https://github.com/bsdlab/dareplane-paper>.

The following different hardware components for signal acquisition and the output of stimulation were used:

- (i) **Arduino** Figure 4 (A) - This rudimentary setup uses an Arduino UNO (Arduino

S.r.l, Monza, Italy) in place of a DBS stimulator. This setup provides an easy-to-replicate benchmark which does not require specialized and expensive hardware components.

- (ii) **BIC-EvalKit** Figure 4 (B) - This setup uses the Brain Interchange (BIC) EvalKit (CorTec GmbH, Freiburg, Germany), a benchtop system which hardware-wise implements a 1-to-1 copy of CorTec's implant. It was chosen as an example of a system that resembles hardware capabilities of an implantable neurostimulator.
- (iii) **Neuro Omega** Figure 4 (C) - This setup uses the CE certified Neuro Omega (Alpha Omega, Alpha Omega Engineering, Nof HaGalil, Israel) system. It represents technically mature systems for stimulation via externalized DBS leads. The technical capabilities of this large research-grade system surpass what currently is possible with commercially available DBS implants. It typically is used intraoperatively or on the ward with patients who have externalized DBS leads.

Raw signal - All tests used a well-controlled 1 Hz sinusoidal source signal with 2 V amplitude, which was generated with the arbitrary wave generator (AWG) of a Picoscope 2204A which has an output frequency of up to 100 kHz. The generated signal was recorded from either the oscilloscope's first channel, (Arduino test) or was provided to the stimulation and recording devices by connecting the oscilloscope probe to the recording channels. When the signal was not recorded with the oscilloscope, additional damping elements of -20dB and -10dB were used in series to lower the amplitude nominally to 2 mV, an admissible range for the CorTec BIC-EvalKit and Neuro

Omega, not driving amplifiers into saturation. The phase shift induced by attenuation can be neglected, since the signal at the oscilloscope probe (after attenuation) is recorded as the ground truth signal with either BIC-EvalKit or Neuro Omega. Any timing difference is always relative to what these devices recorded. The signals were read with individual Dareplane modules streaming data from the hardware-specific APIs and pushing the signal to a dedicated LSL stream. Each module was configured to provide data as quickly as possible to the LSL stream, which leads to an output rate which might differ from the sampling rate when the API provides data in chunks. The internal sampling rates were 500 kHz for the Picoscope (API configuration with sample interval 400 ns and aggregation factor 5) and 5.5 kHz for the Neuro Omega. For the BIC-EvalKit a lower sampling rate aligned with the internal 1 kHz was chosen to avoid the need for upsampling. While the signal recorded with the Picoscope was a single channel only, the full set of 32 channels for the BIC-EvalKit and 16 channels for the Neuro Omega were streamed to LSL.

Decoding - The signal was processed in a mock-up decoding module, which performed reading from the signal LSL stream and pushing data back to an LSL stream for decoded data. This mock-up pass-through decoding was chosen since common decoding methods, such as frequency or spatial filtering, can be computed very efficiently - usually within a few microseconds - leaving the bottleneck for processing with the network communication and memory I/O which are represented by the read and write processes. The target sampling rate for LSL output of the decoding module was set to 2 kHz for the Arduino and Neuro Omega test. Subsampling

for both tests was performed by calculating the median of data received in the $500\ \mu\text{s}$ intervals. For the BIC-EvalKit, which has 1 kHz sampling rate, data was up-sampled by repeating the median of the data buffer (usually one or two samples - see discussion on chunking) to also provide a decoder output with 2 kHz.

Control - Subsequently, a threshold controller picking up the decoded signal, outputting a binary control signal with a numeric value of 150 if the incoming signal was above a predefined threshold or 10 otherwise - the choice of these values is arbitrary. The threshold was chosen to cut the sine wave at approximately half its amplitude of the positive half-wave. This resulted in a threshold at 15000 (equivalent to $1.04\ \text{mV}$) for the experiments with the Neuro Omega. In the case of the BIC-EvalKit, which was used with the smallest possible amplification factor of 37.5, and for the Arduino test, a threshold of 100 (equivalent to $100\ \mu\text{V}$ for the BIC-EvalKit, and $11\ \text{mV}$ for the Arduino test) was used to stay within the same phase of the sinus ($[0, \pi/2]$) as for the other tests.

Stimulation trigger - The controller output was read from LSL by a stimulation module which triggered a single stimulation pulse on the neurostimulators or set the General-Purpose Input Output (GPIO) of the Arduino to high whenever the signal value changed from 10 to 150.

The individual Dareplane modules mentioned above resulted in four different LSL data streams which were used to calculate latencies between the individual processing steps.

ΔSD : time between the raw signal and the out-

put of the pass-through decoder. The time difference was calculated by using the incoming data chunks and their passed through signal. For each chunk, time stamps of the first sample in the signal LSL stream chunk was compared to the first sample of the according chunk in the pass-through stream. Voltage values were compared to ensure correct alignment of samples.

ΔDC : time between the pass-through signal crossing the threshold and the control signals response. The threshold crossing is calculated as the first data sample above the threshold value. The control signals response time was found by selecting the first output value of 150 following a value of 10.

ΔCT : time between the control signal switching to 150 and the control stimulus being sent. The control signal's switch is determined as for ΔCT , while the time of the control stimulus activation is recorded as a single sample of value different from zero.

ΔTS : time between the control signal being sent and the stimulation artifact being visible in the raw signal. The trigger time point is calculated as above while the stimulation artifact is identified in the raw signal by applying a threshold value specific to the stimulation hardware

All three tests were recorded for more than 5 minutes and cropped during analysis to an exact 5 minute sample window to provide consistent sample sizes across the experiments.

2.6. Patient experiment

Readiness for aDBS, i.e., Q3, was assessed within a series of measurement sessions conducted at the Medical Center - University of Freiburg (Department of Stereotactic and Functional Neurosurgery) on a single patient

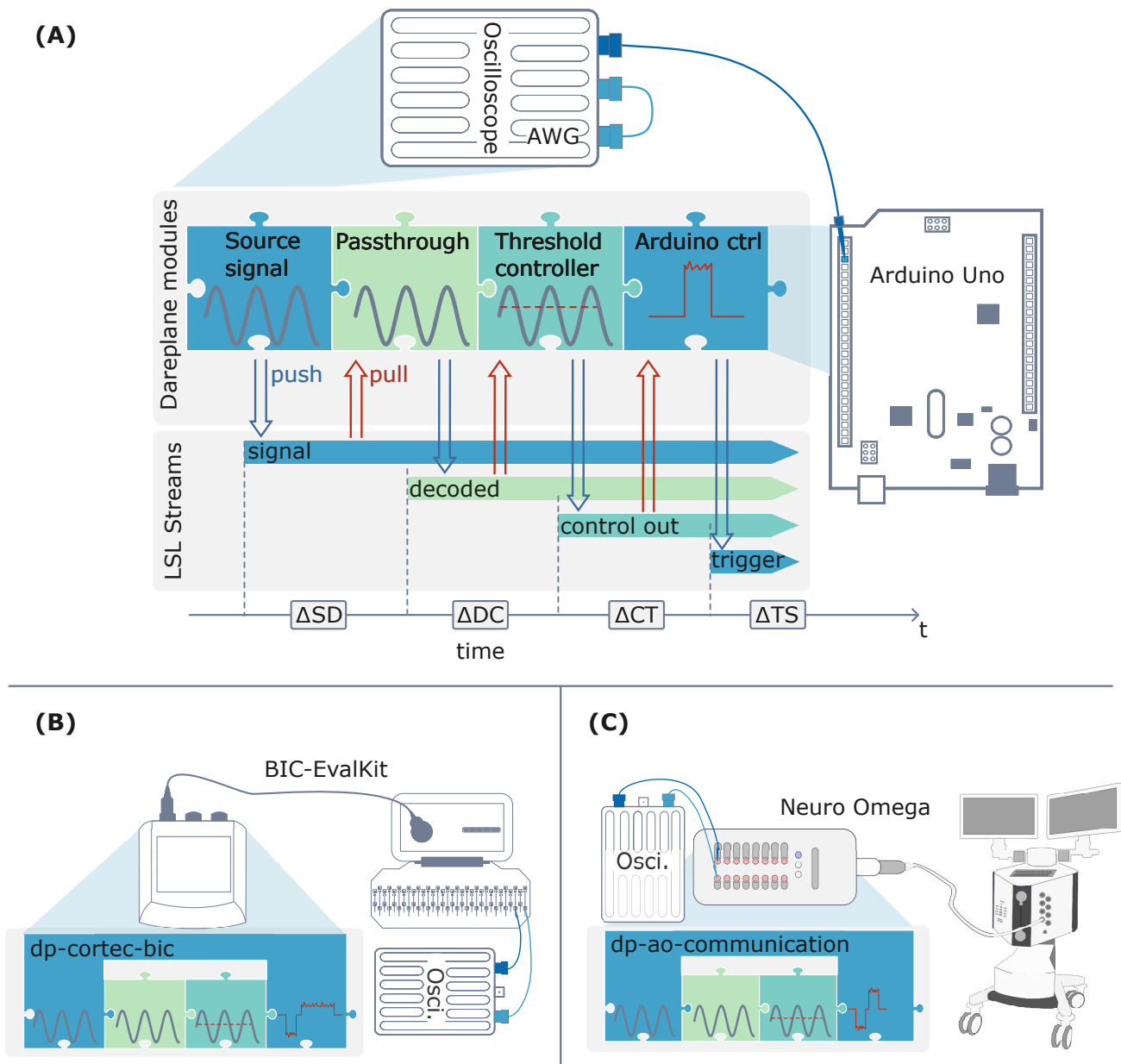


Figure 4: The benchtop setups used for performance testing. (A) shows the setup used for testing with the Arduino Uno as a proxy for a DBS device. The signal input from the AWG of an oscilloscope was read via channel 1 from the oscilloscope while the change of the Arduino's GPIO was tracked via a probe connected to channel 2. The "source signal" from the oscilloscope channels was acquired via API by a Dareplane module which streamed it to a "signal" LSL stream. This stream was picked up by a "passthrough" module which is in place of a decoding module and passes on data without modification to a "decoded" LSL stream. The time stamps from values of the original "signal" LSL stream and the outbound "decoded" stream were compared to calculate ΔSD . A threshold controller Dareplane module picks up the "decoded" signal and outputs a value of 150 if it is above the threshold and 10 otherwise. The timestamp of the first sample above the threshold in the "decoded" stream was compared to the time stamp of the first sample with a value of 150 in the outbound "control_out" stream to compute ΔDC . An Arduino control Dareplane module used serial communication to turn the Arduino's GPIO to high whenever a signal of 150 was incoming and turned it to low otherwise. This module is a placeholder for an actual stimulation device API module. The timestamp of the first value of 150 in the "control_out" stream was compared to the timestamp of the first sample in the "trigger" stream which corresponded to the command of setting the GPIO to high for calculating ΔCT . The final time difference, ΔTS , corresponds to the timestamp difference of the first sample in the "trigger" stream that signaled GPIO high vs the occurrence of the stimulation artifact in channel 2 of the "signal" stream as collected from the oscilloscope. (B) shows the setup used with the BIC-EvalKit with a single Dareplane module for signal collection from the BIC-EvalKits 32 channels, and for sending stimulation commands to the BIC-EvalKit. Both, input and output, had to be combined in a single module as the serial socket only allows for one connection. (C) shows a similar setup as in (B), used for testing with the Neuro Omega. The TCP connection to the Neuro Omega allows only one connection from the client PC, hence a single module is handling signal collection and sending of stimulation commands. Other modules and the evaluation of time stamp differences were the same as for (A).

with PD. The patient (67 years old, female, right-handed) was enrolled in the PD-Interaktiv I study (Extending the Data-Driven Characterization of Neural Markers During Deep Brain Stimulation for Patients with Parkinson’s Disease, DRKS000287039) by providing written consents. This study is ongoing and conducted in accordance with the Declaration of Helsinki and in accordance with local statutory requirements. It was approved by the ethics committee of the Medical Center - University of Freiburg (EK application 21-1545). Participants in the study have the DBS system implanted in a two-stage surgical procedure. In the first stage, Boston Vercise™ (Boston Scientific, Marlborough, USA) directional DBS leads are implanted in the STN (one lead per STN), and are further externalized transcutaneous with special extension wires. An additional four-contact ECoG strip (Ad-Tech Medical Instrument Corporation, Oak Creek, USA) is implanted epidurally over the left primary motor cortex via the same borehole as of the DBS lead. The ECoG strip is also externalized. After implantation and externalization, the patients stay stationary in the ward and take part in the measurement sessions outlined below. In the second surgery, the IPG is implanted, the DBS leads are connected subcutaneously to the IPG, and the ECoG strip is removed.

The first day after the first surgery (i.e., day 1) was dedicated to recovery. On days two, three and four after surgery, measurement sessions, similar to the ones reported in Castaño et al., 2020 [38], took place with the following steps: The patient was brought from the ward to the experiment room. The externalized leads for LFP and ECoG electrodes, and additional four electrooculography (EOG) electrodes were connected to the Neuro Omega (Alpha Omega,

Alpha Omega Engineering, Nof HaGalil, Israel) system which was used to record signals at 22 kHz. Data was streamed using the vendor’s C API and was pushed to an LSL stream for further processing within the Dareplane platform. Additionally, heart rate (HR), respiratory rate (RR) and galvanic skin response (GSR) were recorded on days 2 and 3, using a BrainAmp ExG (Brain Products, Gilching, Germany) system at 5 kHz sampling rate. These modalities were omitted on day 4 for a reduced system load during the closed-loop experiment. After connecting the patient, a titration process was conducted with a clinician to establish the electrode contacts and the maximum amplitude to be used for the given measurement day. A frequency of 130 Hz with symmetric, initial negative pulses of $60 \mu\text{s}$ were used in a monolateral (left or right STN) and bipolar (stimulation and return channel on the DBS lead) stimulation configuration. A bipolar stimulation was chosen as it reduces the amplitude of the stimulation artifact recorded at ECoG electrodes. The stimulation contacts varied between the measurement days and were chosen by the clinician for the subjectively best hand-motor symptom improvement. The configurations during the titration processes are summarized in Table 2, while it is to be noted that during day 2 the stimulation on the left hemisphere was reduced to 4 mA during the first CopyDraw recording block due to the patient reporting a feeling of heat. Once the titration concluded, the actual measurement sessions started with resting recordings of two minutes each, under stimulation OFF, ON (130 Hz). The resting recordings were not analyzed as part of this work.

Next, the main measurements were collected during the CopyDraw [41] task Figure 5 in stimulation OFF and ON blocks in an alter-

Parameter		Day 2	Day 3	Day 4
left	stim. contact	2,3,4	5,6,7	8
	ret. contact	5,6,7	2,3,4	5,6,7
	amplitude	6 mA	6 mA	7 mA
right	stim. contact	8	8	8
	ret. contact	5,6,7	5,6,7	5,6,7
	amplitude	5.5 mA	6 mA	7 mA

Table 2: Configuration of the DBS parameters found during the titration processes conducted on every measurement day. Stimulation frequency (130 Hz) and pulse width (60 μ s) were kept fixed, while a trained clinician selected stimulation and return contacts, as well as amplitude for optimal hand-motor symptom improvement with a bipolar stimulation, separately for the left and right hemisphere. During the CopyDraw experiments on day 2, the stimulation amplitude was reduced to 4 mA in the first recording block with stimulation, due to the patient reporting a feeling of heat. On day 4, a stimulation amplitude of 6 mA was used to stay compatible with day 3, although higher amplitudes were accepted during the titration process.

nating pattern. The patient was thoroughly familiarized with the CopyDraw task one day before surgery to avoid a strong learning curve during the first iterations. During each trial (copy-drawing of one trace), the cursor positions are recorded and nine behavioral features per trial are extracted. The features are velocity, acceleration and jerk, each measured in screen x (horizontal) and y (vertical) directions and as euclidean norm. These features are preprocessed by standard scaling, outlier removal using DBSCAN($\epsilon = 4$) [61] and removal of a linear trend, by fitting and subtracting a linear regression model for each feature. Next, a behavioral score $y_e \in \mathbb{R}$ for each trial e is calculated as the decision function value of a shrinkage regularized [62] linear discriminant analysis (LDA) classification model, which has been trained to predict the stimulation state (ON/OFF) with ON being the continuous open-loop stimulation defined by the clinician. For the purpose of this technical feasibility test, only CopyDraw trials with uninterrupted stylus traces (no pen lift-off during

drawing) were considered to ensure comparable behavioral input. A total of 12 blocks with 12 trials each were collected on each recording day. The block structure started with a stimulation OFF block and then alternated between stimulation ON and OFF.

A 6-fold chronological cross validation was therefore applied to gauge decoding performances, assuring that each adjacent ON/OFF block pair was used as the testing fold once. The area under the receiver operating characteristic curve (ROC AUC) was used to measure the decoding performance of the classifier as folds did become imbalanced when only considering traces without a pen lift-off during the trial. See [41] for details about the CopyDraw task and [38] for an example of how the scores can be used as labels for an EEG decoding pipeline.

To prove the technical feasibility of aDBS with the Dareplane platform, we trained a decoder to predict the CopyDraw scores based on six pre-defined band power features of the ECoG recordings $\mathbf{x}(t) \in \mathbb{R}^{24}$ for data collected on day 3 post-surgery. The ECoG data was collected with ground placed on the right mastoid and referenced to the left earlobe, while the left mastoid was used as reference for additional DBS recordings. A linear regression with L2 regularization, a.k.a., ridge regression model with regularization parameter $\alpha = 1$ from the scikit-learn Python library was used for decoding. The features were extracted per ECoG channel using causal 8th order Butterworth band pass filters within Dareplane decoding module, i.e., using a software filter. The frequency bands were selected as theta (4-8 Hz), alpha (8-13 Hz), lower beta (13-20 Hz), higher beta (20-30 Hz), lower gamma (30-45 Hz) and higher gamma (55-70 Hz). No additional filtering was applied, as the gamma bands did not cover the line

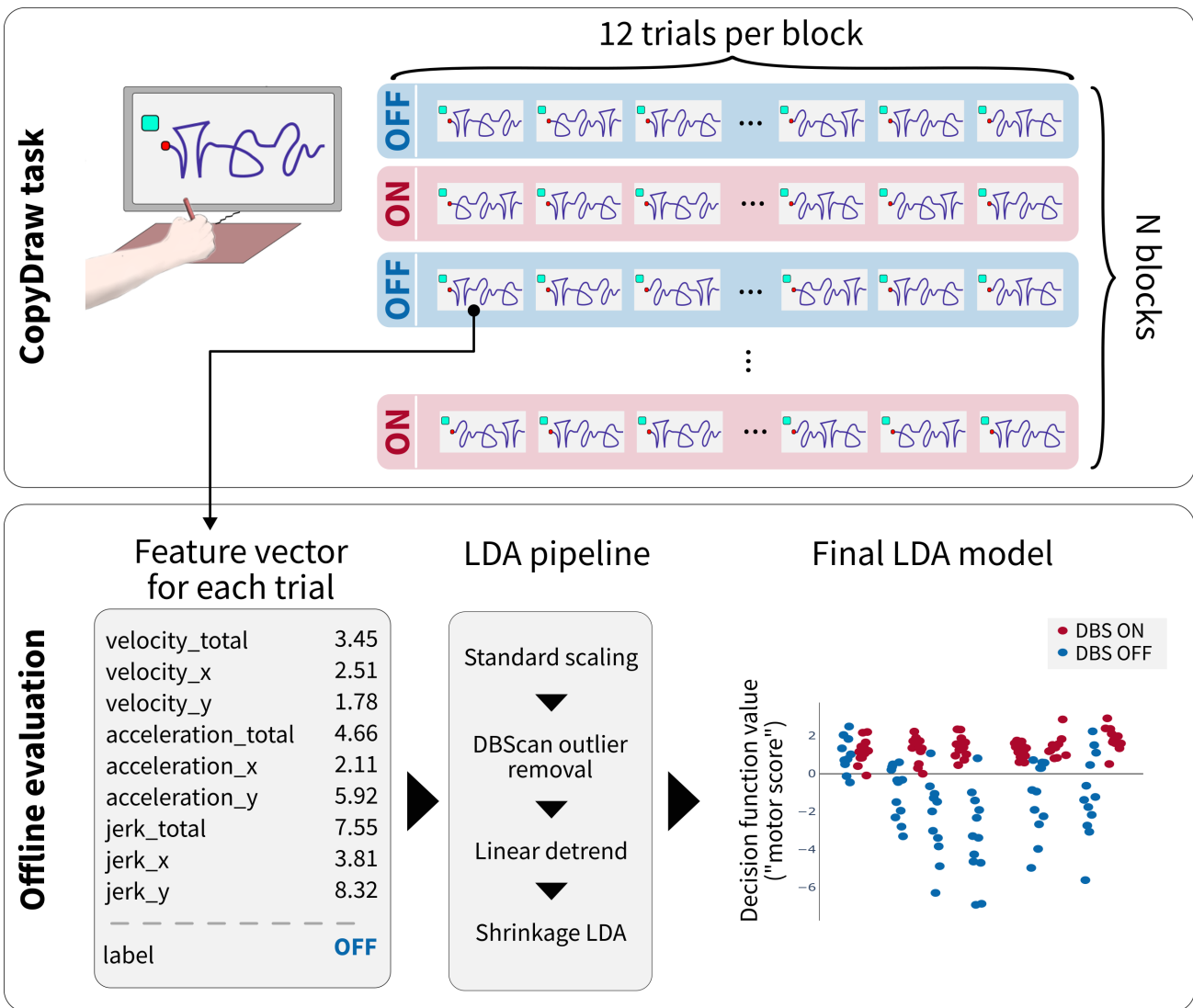


Figure 5: CopyDraw experiment protocol and offline evaluation. The CopyDraw task requires the participant to copy a trace presented on a screen with a stylus on a drawing tablet under time pressure. Twelve trials are collected with a self paced inter-trial-time under a fixed stimulation condition (ON/OFF). Blocks are then collected with iterating stimulation conditions and potential breaks between blocks. After a sufficient number of valid block is collected (usually $N=12$), a model is trained offline to predict the stimulation condition based on nine behavioral features, containing mean velocity, acceleration and jerk, as euclidean norm and individual for the different screen coordinate axes. The features are preprocessed by standard scaling, outlier removal using DBSCAN($\epsilon = 4$) and removal of a linear trend. An LDA model with Ledoit-Wolf regularization is used to predict the stimulation condition. The decision function values of the LDA model are the CopyDraw motor scores, which serve as a proxy for hand-motor performance capabilities. One such motor score is calculated for each trials, i.e., each point in the scatter plot refers to a single trial.

noise artifact at 50 Hz and no stimulation was visible in the spectrum of the ECoG channels below 130 Hz. After filtering the signal, we estimated the band power by averaging over the absolute values of the filtered signal for a given time window. The average for the offline evaluation, i.e., model training with day 3 data, was chosen across a full trial

of CopyDraw of 9s. This trained decoding model was then used on day 4 to provide input to a control module for controlling aDBS - see Figure 6. On day 4, the Dareplane decoding module provided predictions $\hat{y}(t_i)$ of the CopyDraw score at time points t_i with a rate of 5 Hz or 60 Hz. For the online tests (day 4), band power estimates were calculated for

each update interval, disregarding the impact of the smaller averaging window especially on the lower bands for this technical proof of concept. The different update rates were chosen to consider two different load stages for the setup, with 60 Hz being close to the incoming data chunk frequency that was observed during the benchtop tests with the Neuro Omega - see subsection 3.2.

The prediction value $\hat{y}(t_i)$ was then used as the input for a control module, which used a Bollinger band strategy [63] to determine whether to change the stimulation state, motivated by previous work on essential tremor [31]. Bollinger bands are calculated by first computing the moving average of a time series $x \in \mathbb{R}^n$ for a given time window of n_{MA} samples, resulting in $\mu(t_i) = \frac{1}{n_{MA}} \sum_{j=0}^{n_{MA}} x(t_{i-j})$. A sample standard deviation $\sigma(t_i) = \sqrt{\frac{1}{n_{MA}-1} \sum_{j=0}^{n_{MA}} (x(t_{i-j}) - \mu(t_i))^2}$ is calculated for the same window. The window length was 2s. Bollinger bands are then defined as $b^{top}(t_i) = \mu(t_i) + \lambda \cdot \sigma(t_i)$ and $b^{bot}(t_i) = \mu(t_i) - \lambda \cdot \sigma(t_i)$ respectively, with $\lambda \in \mathbb{R}$ being a free parameter, which was set to $\lambda = 2$. Whenever the upper band was crossed ($\hat{y}(t_i) > b^{top}(t_i)$) stimulation was turned off. Whenever the low band was crossed ($\hat{y}(t_i) < b^{bot}(t_i)$) stimulation was turned on, which started stimulation with the target amplitude (6 mA) without ramping. To limit the smallest time window in which the stimulation state could change, a 2s grace period was chosen, in which a stimulation change command would not be processed. Stimulation commands were sent to the Neuro Omega Dareplane module by means of callbacks. The hyper-parameters were chosen arbitrarily to provide reasonable switching times for this technical feasibility test without any other tuning involved.

During the patient experiment on day 4,

a total of 108 CopyDraw trials were collected under aDBS, with 70 uninterrupted (no pen lift-off) trials. Additionally, 24 stimulation OFF and 36 stimulation ON (continuous stimulation) trials were collected, resulting in 15 and 34 uninterrupted trials respectively (Figure 11). The model used on day 4 was trained on all uninterrupted trails from day 3, i.e. $N=43$ for stim OFF and $N=70$ for stim ON.

During the offline data analysis, the decoding quality was assessed by mean Pearson's correlation across the same 6-fold chronological cross validation as was used for the CopyDraw behavioral results. Chance levels were estimated by the 95% quantile of a bootstrapped permutation distribution ($n=2000$). Additionally, an ordinary least squares (OLS) regression fit was performed between predicted and true motor scores, using the statsmodels Python library. Significance of the OLS fitted parameters is assessed by a t-test for the linear dependency with $\alpha = 0.05$ (using the default of statsmodels).

2.7. BCI c-VEP speller

Dareplane also supports setups for more classical non-invasive BCIs. As a prove of feasibility, a c-VEP speller, following the setup of Thielen et al. [64], was implemented on Dareplane to address Q4. A schematic of the setup is shown in Figure 7. Three participants with normal or corrected-to-normal vision participated in the experiments after providing written consent. The c-VEP paradigm [65] displays a keyboard like layout of characters on a screen and simultaneously flashes characters with a unique pseudo-random sequence [66], as implemented in the *dp-cvep-speller* module. Each flash sequence evokes a characteristic brain response which is captured by eight EEG

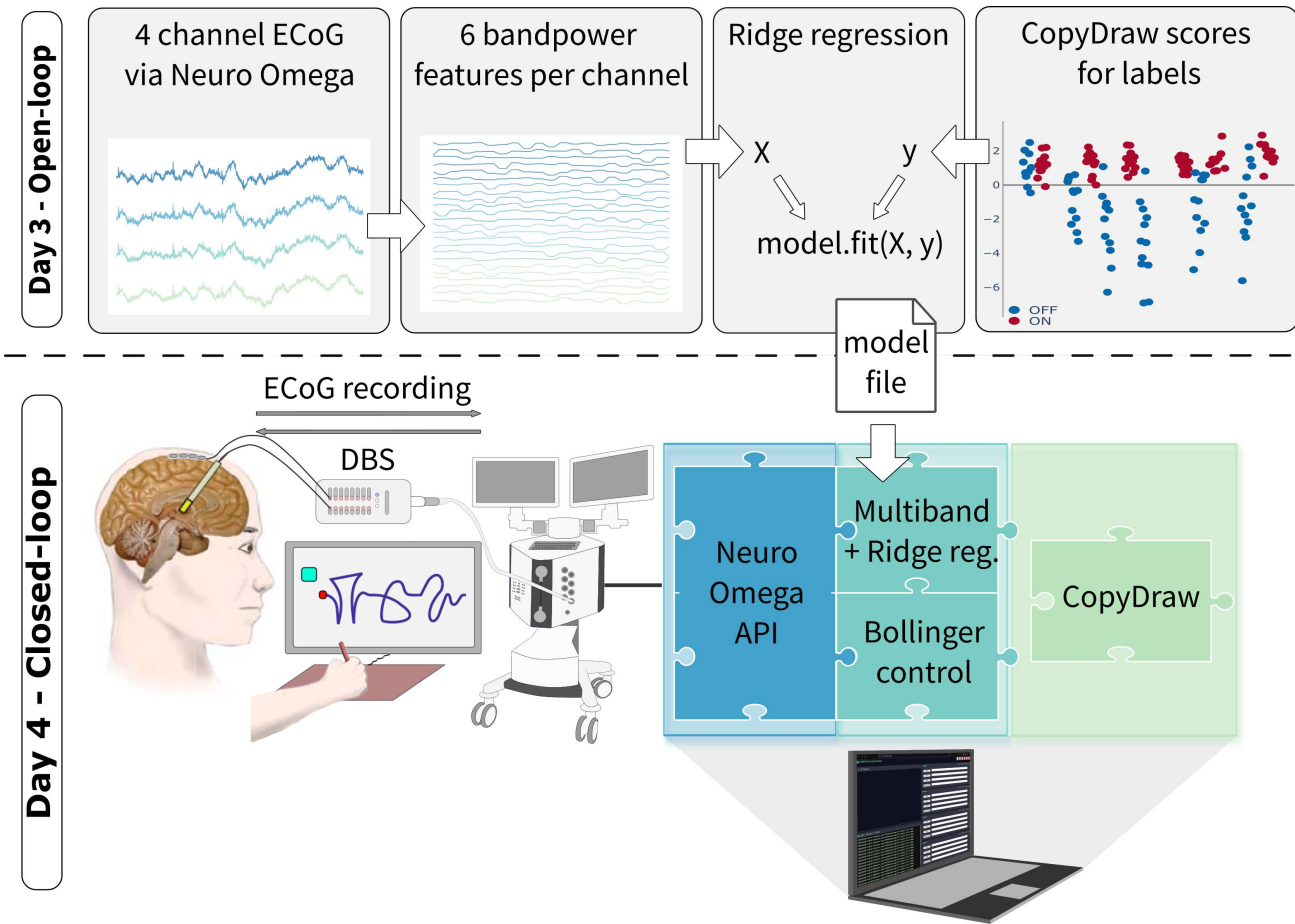


Figure 6: Schematic of the technical feasibility test. The sessions were conducted with a patient with PD which had two DBS leads (implanted over right and left STN) and one 4-channel ECoG (over motor cortex) externalized. Open-loop experiments with the CopyDraw tasks were conducted on the second and third day after surgery. The CopyDraw scores and ECoG data from day 3 were used to train a ridge regression model predicting the CopyDraw scores from bandpower features derived from the ECoG data. This model was then used on day 4 together with a Bollinger band control strategy for providing aDBS via the Neuro Omega.

channels (Fz, T7, T8, POz, O1, Oz, O2, Iz) placed according to the 10-10 system [64]. Data from the training phase is used to train response templates using a reconvolution [67], which was embedded in a canonical correlation analysis (rCCA) [64] that also learns a spatial filter. The training data included 10 cued trials of 4.2s for a total of 42s of training data. The cued targets were selected randomly out of the 63 available cells. During the online phase, the calibrated classifier was applied to single-trials incrementally growing data every 100 ms to allow dynamic stopping according to [64]. At 4.2s a decision is forced by selecting the character with the highest correlation to

a template. Upon classification, feedback for the selection of a letter was provided for 0.7s with highlighting, followed by a 0.3s inter-trial-interval. Each participant completed three runs spelling the target sentence - the quick brown fox jumps over the lazy dog!! - which contains all letters of the alphabet. All missclassifications had to be corrected by selecting the "i" symbol, which performed a backspace. The EEG signals were amplified and recorded using a BioSemi ActiveTwo amplifier recording at 512Hz sampling rate. The raw signal was streamed via LSL and processed in the *dp-cvep-decoder* module. The module continuously bandpass filtered the

EEG data using an 8th order Butterworth bandpass between 6 Hz-40 Hz. The broadband filtered data was then downsampled to 120 Hz, twice the refresh rate of the monitor (60 Hz), which allowed classification with the rCCA [67] approach.

2.8. Scripts and data

All data and analysis scripts are available at the Radboud Data Repository [68].

3. Results

3.1. Dareplane platform

The Dareplane platform is accessible via its github landing page at:

<https://github.com/bsdlab/Dareplane>.

Individual modules are referenced therein. To further enhance accessibility, we provide example modules including a `hello_world` for python and an example in C using SDL2 for paradigm presentation. For recreation of the c-VEP speller setup, a script is provided at <https://github.com/thijor/dp-cvep>.

3.2. Benchtop Results

Arduino test: This relatively simple test revealed the main bottleneck: The control of the GPIO pin showed a mean latency of 12.021 ms, c.f. Table 3. Other modules which are pulling from LSL [58, 59] and pushing to another LSL stream add latency overheads of less than 1 ms on average ($\Delta\text{SD}=0.536$ ms, $\Delta\text{DC}=0.277$ ms, $\Delta\text{CT}=0.335$ ms). The value of the 99% quantile suggest that this performance is overall stable ($\Delta\text{SD}=0.938$ ms, $\Delta\text{DC}=0.543$ ms, $\Delta\text{CT}=0.578$ ms).

BIC-EvalKit test: Similar to the Arduino test case, the bottleneck with the BIC-EvalKit was

found to be the time between sending out the stimulation command and the appearance of the first stimulation pulse in the signal, with a mean latency of $\Delta\text{TS}=22.339$ ms, c.f. Table 3. The other modules showed average latencies of $\Delta\text{SD}=0.793$ ms, $\Delta\text{DC}=0.208$ ms, $\Delta\text{CT}=2.055$ ms on average. The example traces in Figure 8 show an artifact in the sinus wave when readying the system for the next stimulation. The artifact was visible in the whole recording, but was not investigated further as it did not impact the timing measurements.

Neuro Omega test: Again, the bottleneck of the closed-loop response is the time between sending out the stimulation command and the appearance of the first stimulation pulse in the signal. We observed a mean latency of $\Delta\text{TS}=45.961$ ms. Consistent with the Arduino tests, the other modules showed average latencies lower than 1 ms ($\Delta\text{SD}=0.742$ ms, $\Delta\text{DC}=0.331$ ms, $\Delta\text{CT}=0.183$ ms), c.f. Table 3.

Influence of chunking Although the *dp-ao-communication* module was requesting data from the Neuro Omega SDK with a nominal interval of ≈ 500 μs (using a sleep command), analysis of the LSL stream showed that even with the sampling rate of $f_{\text{sample}} = 5500$ Hz being stable, data is incoming in chunks with a mean inter-chunk time of 13 ms [± 4 ms STD] (Figure 9). Chunking affected all streamed sources Table 4. The least chunking was observed for the BIC-EvalKit experiment with an average inter-chunk interval of (2 ± 1) ms which almost met the native 1 kHz sampling rate, followed by the Picoscope (Arduino Uno test) with (7 ± 2) ms, see Figure 9 and Table 4. This chunking has a consequence for various measurements. If, e.g., the time-stamp of

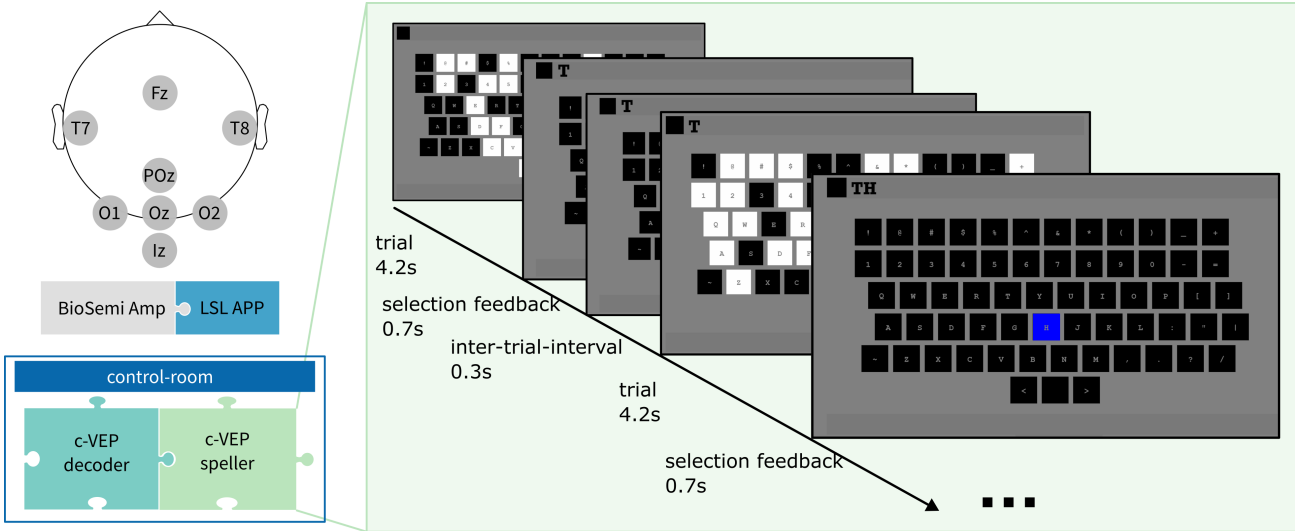


Figure 7: The c-VEP speller setup and paradigm. EEG data is recorded from eight channels using a BioSemi amplifier at 512 Hz streamed to LSL using the BioSemi LSL app. Two Dareplane modules are spawned running the speller paradigm and a decoder using rCCA [67] with early-stopping. The paradigm displays a keyboard layout with $n = 63$ characters, each flashing in a distinct pseudo-random sequence. Trial periods are up to 4.2s, with the possibility for early stopping. During online use, the decoded character is highlighted for 0.7s, followed by a 0.3s inter-trial-interval.

Test type	Difference	Time [ms]					
		mean	min	max	median	q1	q99
Arduino Uno	Δ SD	0.536	0.139	3.268	0.529	0.213	0.938
	Δ DC	0.277	0.095	6.917	0.225	0.119	0.543
	Δ CT	0.335	0.194	0.636	0.322	0.218	0.578
	Δ TS	12.021	0.277	27.736	11.796	8.881	16.456
CorTec EvalKit	Δ SD	0.793	0.532	3.075	0.741	0.569	1.420
	Δ DC	0.208	0.086	2.397	0.197	0.101	0.379
	Δ CT	2.055	1.289	2.871	2.072	1.394	2.819
	Δ TS	22.339	18.543	26.366	22.553	18.612	25.861
Neuro Omega	Δ SD	0.742	0.213	32.546	0.434	0.273	15.859
	Δ DC	0.331	0.092	2.188	0.234	0.105	1.494
	Δ CT	0.183	0.082	1.621	0.153	0.088	0.587
	Δ TS	45.961	28.860	73.765	43.589	32.707	61.458

Table 3: Performance comparison of benchtop system tests, showing mean, min, max, median, 1% and 99% quantiles. Time differences are: Δ SD - signal to decoded, Δ DC - decoded to control response, Δ CT - control response to trigger being sent, and Δ TS - trigger sent to arrival of the stimulation artifact in the signal.

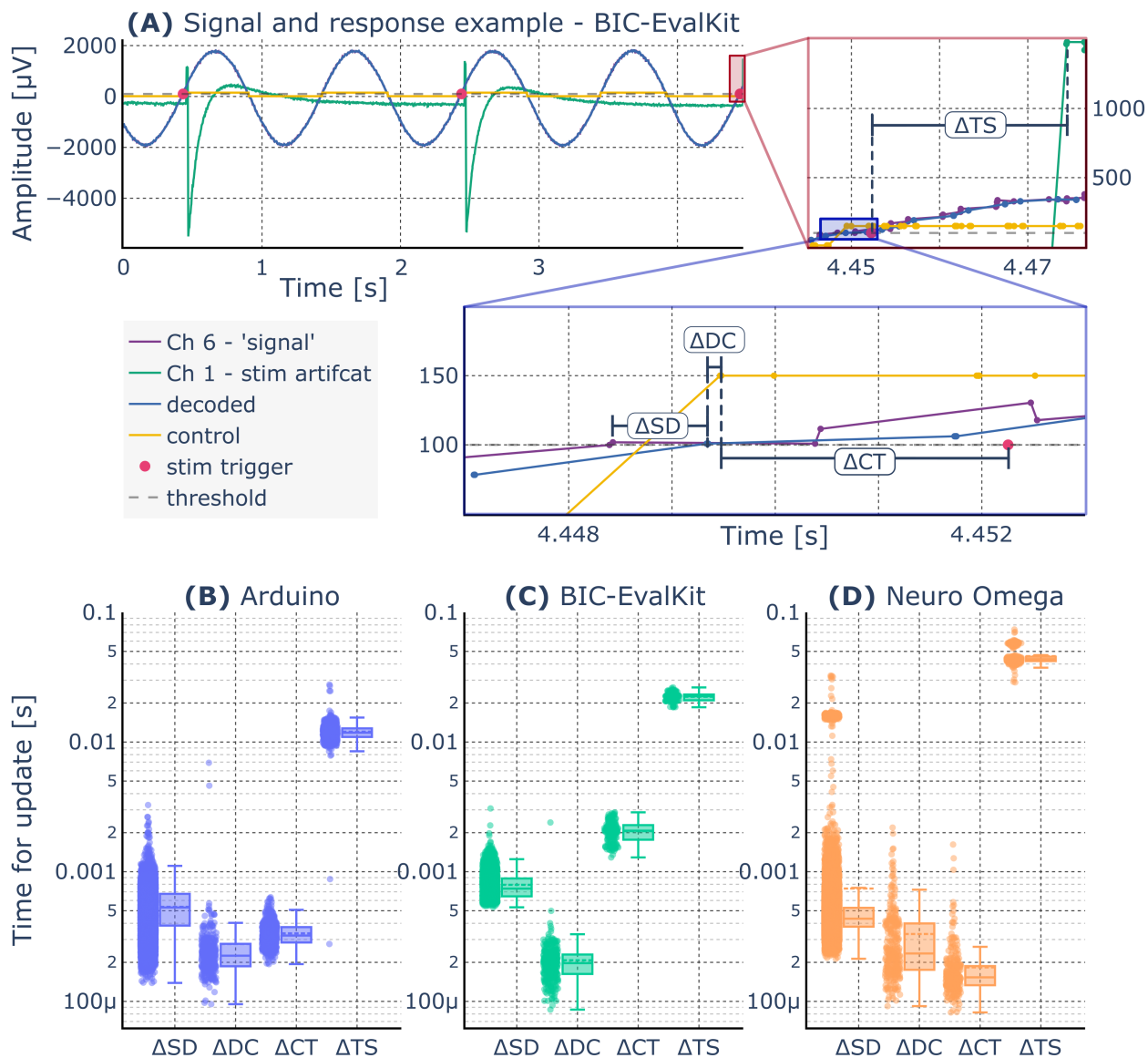


Figure 8: Benchmark performance test results: (A) depicts an example trace of the LSL data streams involved in the BIC-EvalKit testing, showing the 1 Hz sinus which is mostly overlapped by the pass-through decoder output. This is an example of how the closed-loop manifest in the recordings, as the crossing of the threshold at $100\ \mu\text{V}$ off channel six (Ch 6) leads to triggering a single stimulation pulse after passing through the decoding and control modules as visible in the artifact at the channel one (Ch 1). Zoomed in views exemplify how the timing differences were determined. The first zoomed stage (red box) shows how the timing between the stimulation trigger and the stimulation artifact (ΔTS) was determined. The second zoomed stage (blue box) exemplifies how the timing between the incoming signal and the decoder (ΔSD), between the decoder and control output (ΔDC) and between the control output and the stimulation trigger (ΔCT) are determined. The stimulation is triggered by the control modules. (B-D) show box plots of the individual time deltas for the processing steps: ΔSD - signal to decoded, ΔDC - decoded to control response, ΔCT - control response to trigger being sent, and ΔTS - trigger sent to arrival of the stimulation artifact in the signal.

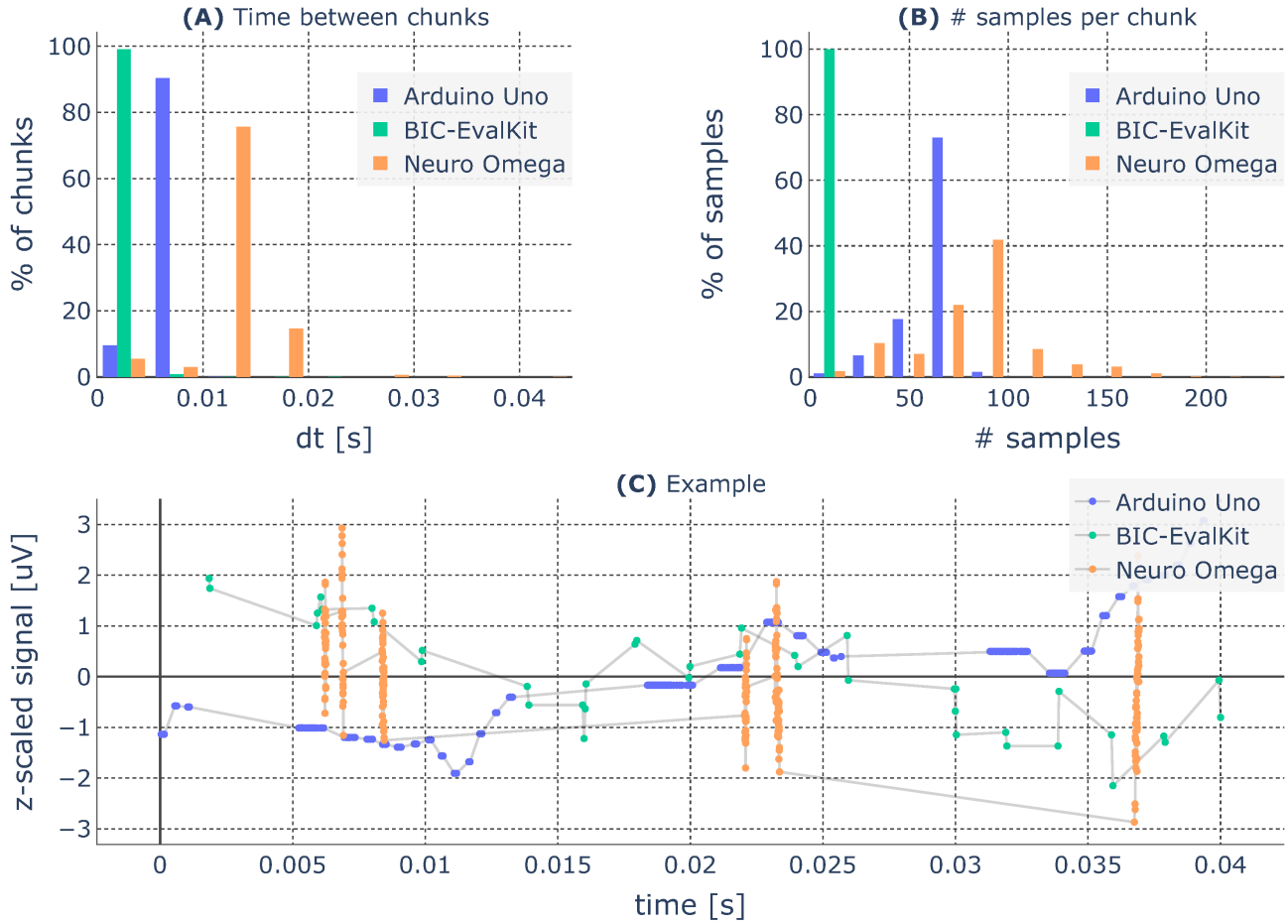


Figure 9: Analysis of chunked data. (A) shows histograms of the time between consecutive data chunks. Chunks were identified by gaps between consecutive sample time stamps ≥ 1 ms. Chunks arrive on average with (13 ± 4) ms for Neuro Omega, (7 ± 2) ms for Picoscope, and with almost no chunking $((2 \pm 1)$ ms) for the BIC-EvalKit. (B) shows histograms of the number of samples within each chunk. (C) shows sample traces from each experiment. Note that the Neuro Omega recorded at 5.5 kHz sampling frequency, resulting in about 80 samples per chunk being processed.

measure	src	mean	std	min	max	q01	q99
dt_chunk [s]	Arduino Uno	0.007	0.002	0.001	0.011	0.001	0.009
dt_chunk [s]	BIC-EvalKit	0.002	0.001	0.001	0.024	0.002	0.004
dt_chunk [s]	Neuro Omega	0.013	0.004	0.001	0.045	0.001	0.029
sample count [#]	Arduino Uno	62.364	12.282	1.000	98.000	19.000	81.000
sample count [#]	BIC-EvalKit	2.313	0.742	1.000	6.000	2.000	4.000
sample count [#]	Neuro Omega	79.697	29.875	1.000	226.000	1.000	163.940

Table 4: Chunking statistics of data recorded in the three benchtop experiments. Rows with measure dt_chunk [s] show aggregates for the time delta between chunks (last to first sample). Rows with measure sample count [#] show aggregates of the number of samples per chunk.

the stimulation artifact within such a chunk is considered for the calculation of ΔTS , the latency is overestimated by at least the

inter-chunk time to the last sample of the previous data chunk. Considering that the relevant time for aDBS is the arrival of the

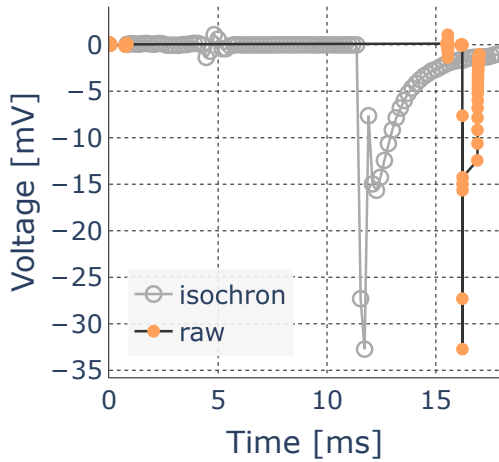


Figure 10: Example of estimating the de-jittered timing of the stimulation pulse. An example of raw data recorded from the Neuro Omega is showing the ≈ 15 ms chunking. Assuming that chunking is caused by data transmission and that the actual samples are recorded with a stable sampling rate, we can estimate the samples of the chunk with time $t_i \pm 15$ ms to lie on an isochron grid following the last sample of the chunk with $t_i \pm 1$ ms. In this isochron approximation, the max value of the stimulation artifact is reached at 11.73 ms compared to the raw signal at 16.22 ms.

stimulation pulse at the neural tissue (t_{stim}) and not the time point when the artifact shows up in the recorded data (t_{rec}), we also calculated the time from sending the stimulation command (t_{cmd}) to a de-jittered stimulation time. For this purpose, we created an isochronous approximation $\hat{t}_{stim} \approx t_{stim}$ of the time when the stimulation pulse was actually delivered. Figure 10 helps to illustrate the approximation. Assume the recorded artifact $t_{rec}^{i,j}$ appears at position j in data chunk i (e.g., raw samples with $t_i \pm 15$ ms in Figure 10) containing n samples with time stamps $[t^{i,1}, \dots, t_{rec}^{i,j}, \dots, t^{i,n}]$. Using $t^{i-1,m}$, the previous time stamp of chunk $i-1$ (e.g., raw samples with $t_i \pm 1$ ms in Figure 10) with m samples, the extrapolated arrival time can then be approximated as $\hat{t}_{stim}^i = t^{i-1,m} + j/f_{sample}$ (under the assumption of a stable sampling rate within the recording amplifier).

Using this corrected \hat{t}_{stim}^i leads to an improved estimate of $\tilde{\Delta}TS$: Mean latencies are reduced from 46 ms on raw LSL samples (using

t_{rec}^i), to 41 ms with the de-jittered time stamps. Such a de-jittered estimation was calculated for the Neuro Omega tests only, as almost no chunking was found for the BIC-EvalKit test, and as the Arduino test is just a proxy domain without the claim of replicating stimulation pulses accurately.

3.3. Patient experiment

The main result of the closed-loop technical feasibility test on the patient with PD is that aDBS was successfully applied and tolerated without side-effects by the patient for continuous windows of more than 20 min (longest window on recording day 4, 11h30 to 11h53). Feasibility was tested during execution of the CopyDraw task and with a decoding model based on the CopyDraw scores collected on day 3. Example traces of the control signal alongside ECoG raw recordings for the aDBS session on day 4 are shown in Figure 12. Whenever the controller input was crossing the Bollinger bands, outside of the grace periods, a stimulation ON or OFF trigger was emitted. The stimulation change is clearly visible by the stimulation artifact appearing or disappearing in all 4 ECoG traces respectively.

The patient showed a clear DBS-induced effect upon the CopyDraw performance, see Figure 11 (A) as an example for day 2. Figure 11 (B) summarizes the stimulation-induced behavioral difference for the two sessions on day 2 and day 3. It shows the mean ROC AUC for a 6-fold chronological cross-validation of the LDA model, 82% for day 2 and 92% for day 3. Please note that no separate evaluation could be conducted for the session on day 4, as the amount of data collected under stimulation OFF and ON conditions was insufficient for this day to fit a comparable LDA model with the same cross

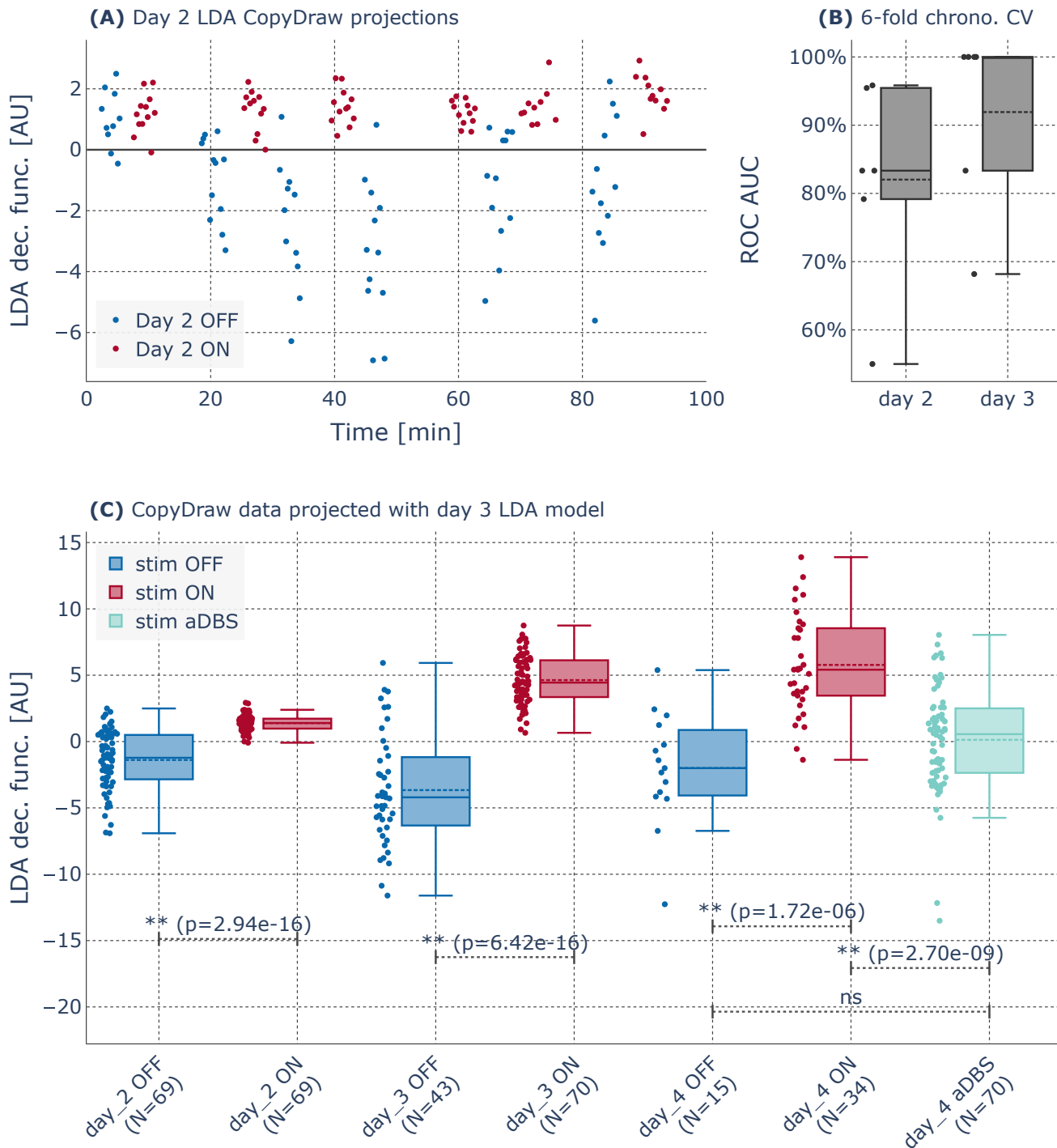


Figure 11: CopyDraw results: (A) CopyDraw scores, i.e. decision function values of a regularized LDA classifier, for individual trials of day 2. The y-axis shows the decision function values, the x-axis time since start of the first trial in minutes. Note that trials with pen lift-off were excluded from analysis, leading to unequal numbers of trials within individual blocks. Furthermore, the projection serves to visualize the stability across time, but is generated from an LDA model fitted on the whole data of this measurement day, such that this cannot be used to interpret generalizability. (B) area under the receiver operating characteristic curve (ROC AUC) for decoding the stimulation state in 6-fold cross-validation respecting chronological order, i.e., always adjacent ON and OFF blocks are considered as test folds. (C) overview of the CopyDraw scores from all three measurement days, predicted with the LDA model trained on day 3 data only. Significance indicators (**) mark test statistics of the Mann-Whitney U test with uncorrected p-values ≤ 0.01 , and *ns* stands for p-value > 0.05 . Horizontal solid lines in the box plots (B) and (C) show median values while dashed lines show mean values.

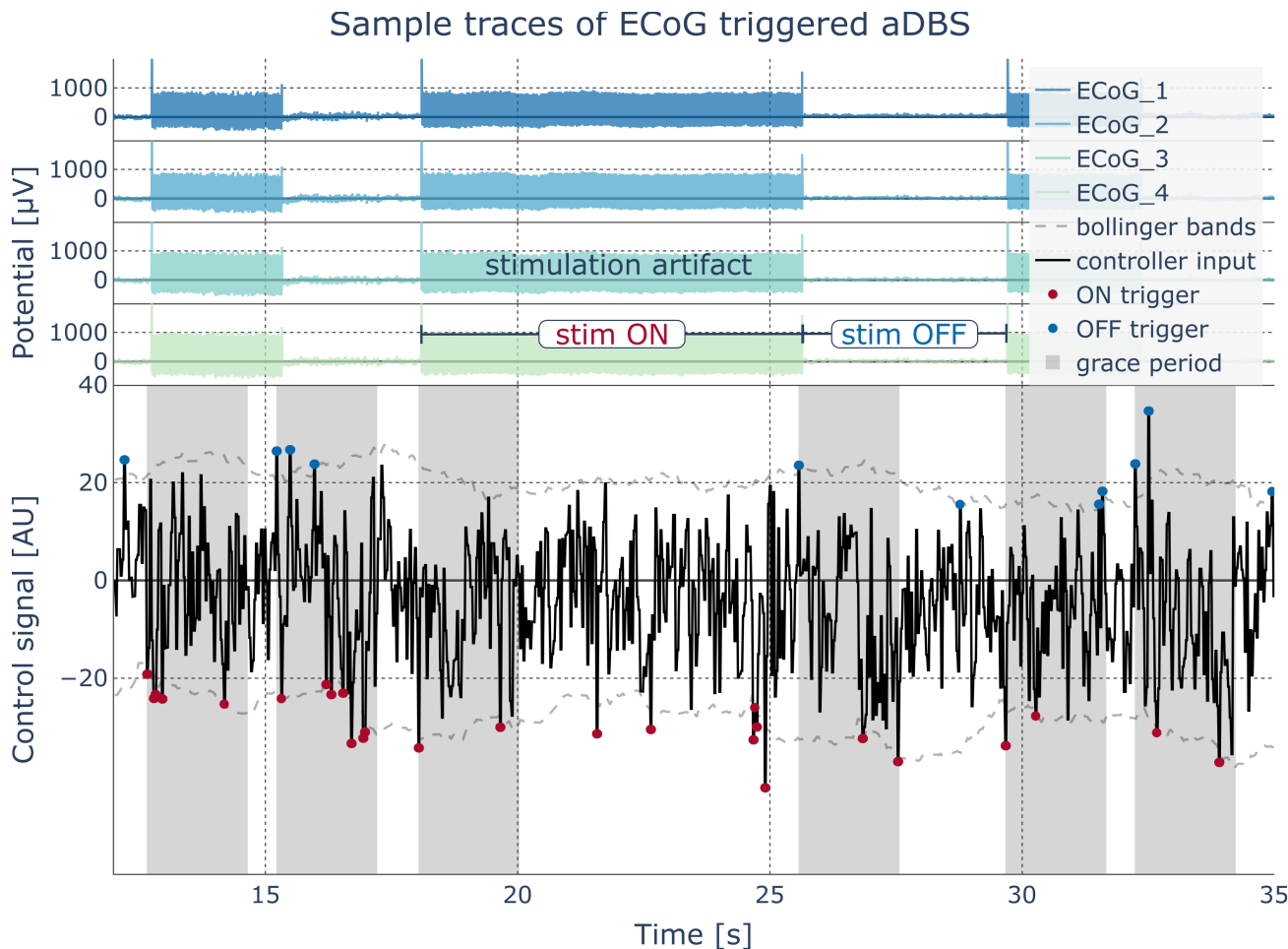


Figure 12: Example traces of the four ECoG channels and the control module data realizing the closed-loop strategy. The first four rows from the top show the ECoG signals, clearly reflecting the stimulation artifact in the stimulation ON segments. The last row shows the input to the Bollinger control module (continuous black trace), the Bollinger bands (dashed gray traces), trigger points (blue for stim OFF, red for stim ON) and grace periods (gray background) following a change of stimulation state. Note that the Bollinger band strategy was selected as it inherently produces crossings on either side of the Bollinger bands, which is an ideal test scenario. This is not a strategy to e.g., optimize the CopyDraw score.

validation procedures.

CopyDraw scores were computed for trials of all three measurement days using the LDA model fitted on the CopyDraw data of day 3, see Figure 11 (C), to validate the stability of this label encoding across the measurement days. The resulting CopyDraw scores are significantly different (Mann-Whitney U test, $P_i < 0.01$) between ON and OFF conditions for all measurement days. The CopyDraw scores obtained under the closed-loop condition (aDBS) are significantly different from the stim ON recordings, but not from stim OFF

recordings obtained on day 4.

Although the decoding quality has not been the objective for this first technical feasibility experiment, a rudimentary analysis of the decoding model is presented in Figure 13. The model coefficients for two models fit on CopyDraw trials of day 3 and trials of day 4 are shown in Figure 13 (A). The scatter plots in Figure 13 (B) and (C) show the CopyDraw scores predicted from ECoG data vs. the (true) CopyDraw scores from the LDA decision function. For Figure 13 (B), prediction results are taken from the 6-fold chronological CV. Mean

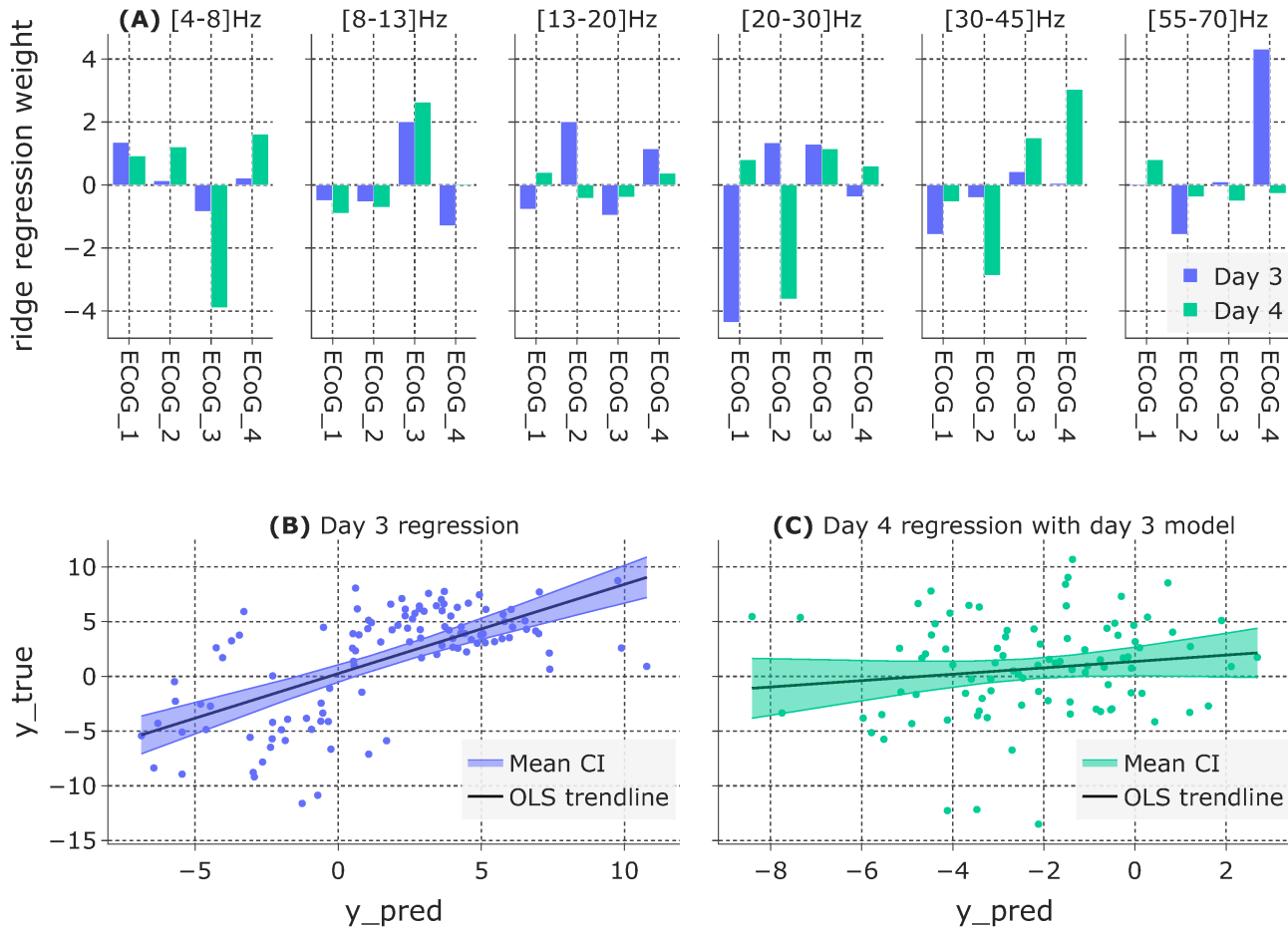


Figure 13: Investigation of the regression model: (A) shows coefficients of the ridge regression model predicting the CopyDraw scores of day 3 and day 4. All CopyDraw scores were derived from an LDA trained on day 3 data only. The models were trained on the full data of each of the days for visualizing the weights. (B) shows the day 3 ridge regression predicted vs actual CopyDraw scores. Predicted scores represent predictions collected during the 6-fold cross-validation. An ordinary least-squares (OLS) trend line was fitted with intercept and is shown with 95% confidence intervals (CI). The slope is significant with $P < 0.01$ while the intercept is not significant $P = 0.51$. (C) is similar to (B) but shows a model trained on all day 3 data to predict CopyDraw scores for day 4. The slope is not significant for the OLS fit with $P=0.17$ while the intercept term is significant with $P=0.04$.

Pearson's correlation across folds is $\rho = 71\%$ (with a chance level of $\rho_{chance} = 21\%$). A linear fit using ordinary least-squares (OLS) shows a significant slope, $P < 0.01$, but no significant intercept parameter ($P=0.51$). For Figure 13 (C), a ridge regression model trained on all data from day 3 was used to produce the predicted scores. The Pearson's correlation $\rho = 14\%$ for day 4 data is below chance level ($\rho_{chance} = 23\%$). An OLS fit shows no significant slope ($P=0.17$) while the intercept is significant ($P=0.04$).

3.4. Other patient experiments conducted with Dareplane

Including the two open-loop sessions and the single open- and closed-loop session (day 4) with the patient referred to above, a total of 19 open-loop DBS sessions were realized using the Dareplane platform. These sessions were conducted with 7 patients with externalized DBS leads, who received DBS treatment for PD or major depression disorder (MDD). See Table 5 for an overview of recorded modalities - the presented patient is PD4. All experiments were conducted with the same

hardware, i.e., the same experiment notebook which was used for the benchtop evaluations. During the 19 sessions, the Neuro Omega system was integrated into Dareplane to record data and provide stimulation. It was controlled via the *dp-ao-communication* module. During the recording sessions, we monitored the LSL signals on a separate notebook to reduce the CPU load of the main experiment notebook. As the module orchestration via the *dp-control-room* uses TCP communication, additional hardware separation would be possible, e.g., by running the paradigm on a dedicated machine. This would however introduce the problem of drifting clocks. A potential resolution would be to either restart or resynchronize the clocks for LSL frequently [69] or, if possible, to use hardware markers that are integrated into the source signal directly. All recording sessions, with the exception of PD4, were purely offline recordings. Data of these sessions is not evaluated here as it would not provide proof of feasibility for the closed-loop processing capabilities.

3.5. c-VEP experiment

All three participants were able to spell the target sentence using the c-VEP interface. The performance metrics for all runs are shown in Table 6. Overall mean values across all subjects show an average correct symbols per minute (CSPM) rate of 13.247, with an accuracy of 90%, an average trial time of 2.712s, and an ITR of 81.942 bits/min. Subject p002 shows the highest average performance with CSPM of 16.522, accuracy of 93%, average trial time of 2.133s, and ITR of 100.296 bits/min. Subject p003 has similar average performance metrics with CSPM of 13.247, accuracy of 91%, average trial time of 2.504s, and ITR of 86.044 bits/min. While

the run (a) of subject p001 shows performance in line with the other subjects, the average performance of p001 is lower with CSPM of 9.227, accuracy of 85%, average trial time of 3.521s, and ITR of 59.485 bits/min.

4. Discussion

4.1. The Dareplane platform

In this work, we have presented Dareplane, a modular and technology agnostic open-source platform for BCI experiments. By pushing the abstraction of the processing steps which are relevant for aDBS research, we have designed the Dareplane platform to stay modular and technology-agnostic. This was realized by using the well-established and -tested LSL [58, 59, 69–71]. Our design resulted in a loose coupling of the modules and overall low requirements on the communication protocol. It is therefore easy to integrate existing software into the platform, e.g., by providing a lean wrapper that processes PCOMMs and interacts with the LSL interfaces. Although there is no preference for functional programming or object-oriented (OO) development philosophies, the Dareplane platform does incorporate the SOLID principles [72] known from OO. They are, however, to be understood on a modular instead of a per-object level. **S**ingle responsibility is realized by defining single modules for each processing step. The **O**pen-closed principle is realized, as the platform is open for extensions by adding new modules, and closed to modification, as these new modules can be added without the need to change existing modules. **L**iskov substitution can be understood as replacing modules for a given task in an existing setup, e.g., by replacing the behaviour paradigm or the algorithm used for decoding. **I**nterface segre-

Patient	$N_{sessions}$	Modalities (channel count)	
		22 kHz sampling	5 kHz sampling
PD1	3	LFP(16), ECoG(4), EOG(4)	HR(1), RR(1), GSR(1)
PD2	3	LFP(16), ECoG(4), EOG(4)	HR(1), RR(1), GSR(1), EEG(85) last session only
PD3	3	LFP(16), ECoG(4), EOG(4)	HR(1), RR(1), GSR(1)
PD4	3	LFP(16), ECoG(4), EOG(4)	HR(1), RR(1), GSR(1) - only in session 1 and 2
MDD1	3	LFP(16), ECoG(4), EOG(4)	HR(1), RR(1), GSR(1)
MDD2	2	LFP(16), ECoG(4), EOG(4)	HR(1), RR(1), GSR(1)
MDD3	2	LFP(16), ECoG(4), EOG(4)	HR(1), RR(1), GSR(1)

Table 5: Overview of recordings conducted with Dareplane experimental setups at the UMC Freiburg. The presented CopyDraw evaluation and the closed-loop feasibility test refer to patient PD4. All other measurements were pure offline recordings. Recordings via the Neuro Omega were collected at 22kHz while recording via the BrainAmp ExG were collected at 5kHz. Heart rate (HR), respiratory rate (RR), and galvanic skin response (GSR) were collected using the according BrainAmp ExG sensors, while EEG was recorded using a BrainAmp with a gel based passive BrainCap (Brain Products, Gilching, Germany). HR, RR and GSR were not recorded during the closed-loop experiment to reduce the load on the experiment notebook.

Subject	Run	CSPM	Accuracy	Average trial time [s]	ITR [bits/min]
p001	a	11.105	91%	3.423	67.988
p001	b	9.376	85%	3.412	60.402
p001	c	7.198	78%	3.728	50.065
mean _{p001}		9.227	85%	3.521	59.485
p002	a	14.829	91%	2.268	91.149
p002	b	17.291	94%	2.048	104.407
p002	c	17.444	94%	2.021	105.332
mean _{p002}		16.522	93%	2.113	100.296
p003	a	15.089	94%	2.495	91.055
p003	b	11.652	85%	2.547	75.137
p003	c	15.240	94%	2.469	91.940
mean _{p003}		13.994	91%	2.504	86.044
mean_{all}		13.247	90%	2.712	81.942

Table 6: Overview c-VEP speller experiments. The information transfer rate (ITR) is including a 1 s inter-trial-time. CSPM stands for correct symbols per minute.

gation is inherent, as each module only provides PCOMM functionality specific to itself, and only queries LSL streams specified for its own use. Lastly, **D**ependency inversion, which is also understood as depending on abstractions instead of concretions, was the core idea behind Dareplane’s design.

The above-mentioned features were achieved

at the expense of 1) a network communication overhead and 2) a memory overhead induced by every module having its own data buffers, and 3) the platform targeting a tech-savvy user group. Both, 1) and 2) are caused by the independence of each module and the data streaming via network communication.

This is mainly a constraint to consider dur-

ing the design process of a setup, and users should be aware of how much data is streamed, which usually is not a problem in the BCI context, with the potential exception of high frequency video data [58], or invasive single-unit activity recordings with high sampling rates and large channels counts. The same holds for the buffer design, which is a trade-off between the necessary data history and the available memory. However, this does not affect the permanent data recording, as raw signals and LSL streams can be written to hard-drive in parallel. Furthermore, each module will be spawned in a separate subprocess. Depending on the module, it will include a kind of `main loop`, presenting a continuous CPU load which might exhaust the hardware capabilities. As the benchtop tests reveal, it is still possible to support high throughput with modest consumer-grade hardware, as opposed to other similar solutions which are further optimised for performance [51], but require large amounts of memory or CPU power to achieve this performance.

Although Dareplane targets a technically versed user group, the platform is still very accessible, provided a user is proficient with the programming language they chose to implement their own modules with. Reusing existing modules based on, e.g., Python, requires the user to understand how to set up and manage python programming environment.

While the current Dareplane modules use LSL [58] for data streaming, there is no strict dependency on it. Modules could be implemented with other streaming technology or even allow for configurable streaming backends.

Compared to mature and feature rich platforms like BCI2000 [47], Dareplane, in its current state, provides less functionality

out of the box. With its design of minimal requirements, implementing new functionality should however be made very accessible. E.g., working purely with interpreted software is possible, while compiled code can be used wherever needed for communication with APIs or when performance critical components should be optimized. Furthermore is Dareplane usable on UNIX and Windows systems alike, while platforms like BCI2000 can face functional constraints when being compiled for non Windows systems. Cross platform availability is of course easier for younger platform projects. Supporting just Windows might not be a downside however, especially when also targeting a user group that is not developing custom software for their experiments.

4.2. Benchtop tests

Observed latencies - The latency and performance benchtop tests conducted with modest hardware have revealed the general possibility of processing data at high rates ≥ 1 kHz in the Dareplane platform. Regarding latencies, we have identified the comparably slow responses of the stimulation hardware based on API triggers as the key bottlenecks for a closed-loop system. Other platforms have considered a closed-loop performance as feasible, if round-trip times of less than 15 ms [50, 51] can be achieved. These thresholds were considered for pure on-platform processing or by recording a digital output signal, but did not consider a delay by a potential feedback device, such as a neurostimulator or the refresh of a screen. Our benchtop test showed that, if omitting the stimulation device's response for a fair comparison, the Arduino ($\Delta_{q99}SD + \Delta_{q99}DC + \Delta_{q99}CT = 2.059$ ms) and BIC-EvalKit ($\Delta_{q99}SD + \Delta_{q99}DC + \Delta_{q99}CT =$

4.618 ms) tests stay below this value for the sum of their 99% quantiles. The processing time for the Neuro Omega can be slightly above this value ($\Delta_{q99}SD + \Delta_{q99}DC + \Delta_{q99}CT = 17.941$ ms), which is mainly caused by the pass-through time of data that is chunked in different clusters, which is clearly visible by the $\Delta_{SD} \leq 10$ ms values of Figure 8 (D). This leads to $\Delta_{q99}SD$ values around 16 ms.

The results for the simplified Arduino test lead to a question as the observer (Arduino mean GPIO reaction ΔTS) is much slower than observed GPIO response times of less than 1 ms [73] with a comparable LSL setup. A direct comparison, however, is not possible as the Arduino used in the experiment by Appelhoff et al. [73] was programmed differently, also using a higher baud rate for the serial communication. Still, a systematic delay in the timestamps received from the oscilloscope module or API could be another explanation for the observer difference. A separate calibration procedure with the oscilloscope module will be necessary to rule out a systematic delay and will be part of future investigations.

The delay observed between crossing the signal threshold and the appearance of the stimulation artifact 20-40 ms later for the BIC-EvalKit and Neuro Omega is in line with delays reported by other groups stimulating on externalized leads [22, 74]. Whether this delay can be considered a sufficient latency depends on the use case. Given the long-tailed distribution and the occasional outlier with very long timestamp differences, it is clear that a Dareplane setup cannot provide tight timing guarantees running on a regular operating system.

Dareplane provides only "soft real-time" [75] capability, which means that there is no guarantee for a processing step to be exe-

cuted within a given time window. This characteristic is shared by other platforms running on regular operating systems. Only dedicated platforms for hard realtime processing are capable to provide guaranteed processing [75]. Considering the processing windows of current aDBS applications, which usually comprise a processing every few 10-100 ms [22, 24, 76] or even adjusting stimulation only once per second [77], the latencies achieved with Dareplane seem to be sufficient to realize similar protocols nonetheless.

Time-critical markers for aDBS - Looking forward, a very recent proposed approach to aDBS is based on beta-burst predictive triggering [78]. The authors used a neural-network classifier to predict the occurrence of beta bursts [79], for which a reliable classification was achieved between 30-80 ms prior to burst onset [78]. A response within this time window would be possible using the tested hardware.

Another marker discussed for aDBS of patients with PD is phase-dependent stimulation [80], which is common in essential tremor where the frequency used as a biomarker typically is in the slower theta (5-8 Hz) range [81]. Furthermore, the neural oscillation is tightly coupled to the tremor frequency, allowing, e.g., an aDBS system based on accelerometric data [31]. Using the phase of a narrow-band oscillation in the context of PD as a marker for aDBS is to our knowledge only applied in animal models [82] and discussed with simulation models of the thalamo-cortical system [83]. Triggering stimulation phase-dependent on the beta oscillations is an interesting and technically challenging potential future use case for the Dareplane platform.

Timing uncertainty - It is informative to also compare the measured latencies to signal-specific timing metrics to judge if latencies induced by the modular Dareplane structure are acceptable. For LSL streams of different hardware sources, timing can be analysed regarding fixed offsets, drifts and jitter. Fixed offsets are accounted for by LSL and are usually in the range of 10 ms [58]. Drifts caused by different hardware clocks are observed to be around 0.03 ms/s [69,70] and can have a severe impact on decodability [69]. Finally, jitter is observed to be around 1.7 ms [69, 70]. For BCI systems based on evoked responses, jitter values of 10 ms and larger lead to a significant SNR reduction [84]. Given these independent timing inaccuracies, we consider the overhead introduced by the modular structure of the Dareplane platform acceptable.

Data arriving in chunks provides another timing uncertainty that may compromise closed-loop response times. Receiving data in chunks rather than on a per sample basis is hardware-specific and is also to be expected for other signal recording hardware [48] including IPGs [76].

Load restrictions - While testing the benchtop setups, the standard Windows system monitor showed total CPU usages larger than 90 % when the modules were configured with higher sampling rates, e.g., processing modules operating at 1 kHz on data from the Neuro Omega at 22 kHz for 24 channels. We empirically observed data loss whenever the system was above a CPU load of 95 % for more than a few seconds. This implies that whenever a demanding decoding method is considered, either a slower sampling rate (within the modules) needs to be selected, or more potent hardware should be used. Given the modular nature of the setup, which spawns separate processes for

each module, we expect robust performance increases by the kill-it-with-iron approach of facilitating more cores.

Comparability of the setups - Comparing the three benchtop tests it is interesting to note that the time delay between the LSL timestamp for triggering a stimulation and the arrival of the stimulation artifact of the Arduino Uno GPIO $\Delta_{TS}^{AUno} = 12$ ms is at least roughly comparable to the latencies achieved with the Neuro Omega system $\Delta_{TS}^{NO} = 46$ ms or CorTec’s BIC-EvalKit $\Delta_{TS}^{BIC} = 22$ ms. This suggests that realistic benchtop experiments can be created with low-cost, accessible hardware, which allows to pre-test setups when access to the clinical hardware is limited, or would allow to realize student projects under financial constraints.

4.3. Patient experiments

Regarding the feasibility of Dareplane to perform an aDBS experiment with a patient in the loop, we can conclude that it was technically feasible to use the Dareplane platform for a aDBS experiment. The achieved update cycles with up to 60 Hz are comparable to update speeds in current aDBS experiments, ranging from 2 Hz [24] to a few 10 Hz [76]. The resulting stimulation pattern was tolerated well by the patient for extended stimulation periods, which were similar in length to time windows reported by other studies with stimulation on externalized leads [25]. The chosen control strategy aimed to ensure that a switching of the stimulation was triggered in order to run a technical feasibility test of the closed-loop functionality. We did not aim to find the optimal control strategy that would result in the best CopyDraw performance, or would even lead to a clinically

optimal symptom improvement. The resulting CopyDraw scores observed on day 4 during the aDBS session are not significantly different from stimulation OFF blocks of the same day. It is to be noted that the CopyDraw score by design leads to an optimized discrimination between stimulation ON and OFF. It does not describe the quality of the copied trace as such. It is therefore possible that an objective rater would judge the quality of the CopyDraw traces produced by the patient during stimulation OFF state as higher than traces produced during the ON state. Overall, the stimulation effect on the CopyDraw score was stable across all three measurement days, as can be seen by the significant difference of the stimulation ON vs. OFF blocks from just one LDA model (see Figure 11). Having such a stable behavioral effect, paired with the high ROC AUC scores for of the CopyDraw LDA models for day 2 (82%) and day 3 (92%) is not common for patients with PD performing CopyDraw [38]. The labels therefore provided high contrast information for the neural decoding. This is in line with the high correlation achieved by the ridge regression used with the ECoG multi-band features of day 3. Contrary to the behavioral decoding, the transfer of the ridge regression model for neural decoding did not generalize to the different day 4 – a significant correlation could not be achieved between the predicted and the actual CopyDraw scores. This potentially indicates that neural markers for the CopyDraw performance are unstable over days, which is also reflected in the very different ridge regression weight distributions between both days. It is to be noted however, that these regression weights are difficult to interpret, as a large weight could either be related to a strong signal or a component to average out noise [85]. Furthermore,

while unstable markers indicate the need for session-specific marker identification known from EEG data [38], most trials (N=70, Figure 11(C)) on day 4 were conducted under an aDBS condition. The impact of such a changed stimulation protocol upon the decoding performance of CopyDraw is unknown and needs to be subject of further investigations. Explicitly, no LDA model for day 4 could be trained as there was an insufficient number of trials under pure stimulation ON and OFF collected, in favor of performing more blocks under aDBS. Thus no ROC AUC for the CopyDraw was reported for day 4. Another limitation of the presented proof of concept is that the decoding approach was not exhaustively investigated. Including band-power features beyond 70 Hz or a different binning of the bands could improve the decoding performance. Furthermore, the used moving-average approximation for the band-power is only a cost efficient, but potentially crude approximation which could be optimized by considering the variance of the (narrow) band-filtered signal, or a Hilbert transform in a causal filter design for allowing comparability to online decoding. Additionally, a different choice for ground and reference, e.g., using one of the ECoG channels, should be considered to reduce noise and correlation in the signal.

4.4. *c-VEP experiments*

The performance metrics of all three participants with mean ITR of 81.942 bits/min, are similar to the published results for the rCCA decoding approach [67] with early stopping [64]. While using a different keyboard grid with only n=29 characters, Thielen et al. [64], report an average ITR of 67.9 bits/min (max. 106.7, min. 44.2) for the copy-spelling

task. With this successful replication of the c-VEP speller on three healthy participants, we demonstrate the use case of Dareplane for a non-invasive BCI. With the provided setup script, we hope to foster adaptation of the Dareplane platform, as replicating the experiment requires a setup available in many labs: an LSL integrated EEG system, a screen for stimuli presentation, and a PC for running the software.

4.5. Future development

The presented Dareplane setups were all hosted on a single machine. Given the general capability of running on distributed systems, an interesting next step would be to consider a setup involving at least two machines with simultaneous processing tasks. While performance measurements exist for the use of multiple machines for data acquisition and processing [84, 86], it is not clear how distributing decoding and/or control strategies tasks over different machines would impact the overall latency. The results of the performance benchmark presented in this paper are to be understood as an out-of-the box potential with modest hardware. A more comprehensive benchmarking could consider more potent hardware, or the optimization of individual modules, e.g., by aligning the update cycles of the main loops of individual modules. Finally, an evaluation using a network stack in combination with a realtime operating system could provide interesting insights into how far the modularity in combination with LSL for data communication can be pushed.

5. Conclusion

While the decoding of biomarkers for closed-loop neurotechnology systems like BCIs and

aDBS is a very active research topic, the problem of optimizing adaptive stimulation seems to be harder and so far is addressed by few publications only. The reason for this may partially be explained by a lack of a versatile aDBS software platform. With Dareplane, we have developed and offer an open-source modular software platform to the community for running BCI- and specifically aDBS experiments. The platform uses TCP communication for exposing and triggering functionality and uses LSL for sharing and recording of data. Dareplane’s tech-stack is mostly technology agnostic and allows integrating existing code with very little overhead. The conducted benchmarks show a sufficient latency for most BCI and aDBS tasks. We tested the technical feasibility for aDBS in a clinical experiment with a single patient with PD and demonstrated its general applicability in a non-invasive c-VEP BCI application. As an open-source project, we hope to steadily grow the platform and improve quality and functionality with a wider range of developers and contributors in the long run.

Acknowledgments

MD receives funding from the Dareplane collaboration project, which is co-funded by PPP Allowance awarded by Health Holland, Top Sector Life Sciences & Health, to stimulate public-private partnerships as well as by a contribution from the Dutch Brain Foundation. The Dareplane project also received in kind contributions by CorTec (Freiburg, Germany) and Newronika (Milan, Italy). JP is funded by the Deutsche Forschungsgemeinschaft (DFG) under the Walter Benjamin Programme (Project number 510112977). The PD-Interaktiv I study is funded by the Bun-

desministerium für Bildung und Forschung (Grant 16SV8011). BS receives a research grant from Ceregate (Hamburg, Germany) and honoraria as an advisor for Precisis (Heidelberg, Germany), both unrelated to this work. VC receives a collaborative grant from BrainLab (Munich, Germany). He serves as an advisor for Aleva (Lausanne, Switzerland), Ceregate (Hamburg, Germany), Cortec (Freiburg, Germany) and Inbrain (Barcelona, Spain). He has an ongoing IIT with Boston Scientific (USA). He has received travel support and honoraria for lectures from Boston Scientific (USA), UNEEG Medical (Munich, Germany), and Precisis (Heidelberg, Germany).

Author contributions

MD: Platform design and development, conducting patient experiments, implementation c-VEP speller, writing original draft. **JP:** Platform design and development, open-loop patient experiments. **JT:** implementation c-VEP speller, conducting cVEP speller experiments. **MT** and **MJ:** Platform design. **BS** and **VC:** Patient recruitment, surgery, and safety surveillance during experiments. **All authors:** Writing - review & editing.

References

- [1] Society B. BCI definition; 2024. Accessed: 13th June 2024. <https://bcisociety.org/bci-definition/>.
- [2] Hofmann UG, Stieglitz T. Why some BCI should still be called BMI. *Nature Communications*. 2024 Jul;15(1):6207. Available from: <https://doi.org/10.1038/s41467-024-50603-7>.
- [3] Krauss JK, Lipsman N, Aziz T, Boutet A, Brown P, Chang JW, et al. Technology of deep brain stimulation: current status and future directions. *Nature Reviews Neurology*. 2021 Feb;17(2):75-87. Available from: <https://doi.org/10.1038/s41582-020-00426-z>.
- [4] Najera RA, Mahavadi AK, Khan AU, Boddeti U, Del Bene VA, Walker HC, et al. Alternative patterns of deep brain stimulation in neurologic and neuropsychiatric disorders. *Frontiers in Neuroinformatics*. 2023;17. Available from: <https://www.frontiersin.org/articles/10.3389/fninf.2023.>
- [5] Sellers KK, Cohen JL, Khambhati AN, Fan JM, Lee AM, Chang EF, et al. Closed-loop neurostimulation for the treatment of psychiatric disorders. *Neuropsychopharmacology*. 2024 Jan;49(1). Available from: <https://doi.org/10.1038/s41386-023-01631-2>.
- [6] Groppa S, Gonzalez-Escamilla G, Tinkhauser G, Baqapuri HI, Sajonz B, Wiest C, et al. Perspectives of Implementation of Closed-Loop Deep Brain Stimulation: From Neurological to Psychiatric Disorders. *Stereotactic and Functional Neurosurgery*. 2023 12;102(1):40-54. Available from: <https://doi.org/10.1159/000535114>.
- [7] Wu H, Hariz M, Visser-Vandewalle V, Zrinzo L, Coenen VA, Sheth SA, et al. Deep brain stimulation for refractory obsessive-compulsive disorder (OCD): emerging or established therapy? *Mol Psychiatry*. 2020 Nov;26(1):60-5. Available from: <https://doi.org/10.1038/s41380-020-00933-x>.
- [8] Coenen VA, Schlaepfer TE, Goll P, Reinacher PC, Voderholzer U, Tebartz van Elst L, et al. The medial forebrain bundle as a target for deep brain stimulation for obsessive-compulsive disorder. *CNS Spectr*. 2016 Jun;22(3):282-9. Available from: <https://doi.org/10.1017/s1092852916000286>.
- [9] Mayberg HS, Lozano AM, Voon V, McNeely HE, Seminowicz D, Hamani C, et al. Deep brain stimulation for treatment-resistant depression. *Neuron*. 2005;45(5):651-60. Available from: <https://doi.org/10.1016/j.neuron.2005.02.014>.
- [10] Kisely S, Li A, Warren N, Siskind D. A systematic review and meta-analysis of deep brain stimulation for depression. *Depress Anxiety*. 2018 Apr;35(5):468-80. Available from: <https://doi.org/10.1002/da.22746>.
- [11] Coenen VA, Bewernick BH, Kayser S, Kilian H, Boström J, Greschus S, et al. Superolateral medial forebrain bundle deep brain stimulation in major depression: a gateway trial. *Neuropsychopharmacology*. 2019 Mar;44(7):1224-32. Available from: <https://doi.org/10.1038/s41386-019-0369-9>.
- [12] Alagapan S, Choi KS, Heisig S, Riva-Posse

- P, Crowell A, Tiruvadi V, et al. Cingulate dynamics track depression recovery with deep brain stimulation. *Nature*. 2023 Oct;622(7981):130-8. Available from: <https://doi.org/10.1038/s41586-023-06541-3>.
- [13] Cagle JN, Okun MS, Cernera S, Eisinger RS, Opri E, Bowers D, et al. Embedded Human Closed-Loop Deep Brain Stimulation for Tourette Syndrome: A Nonrandomized Controlled Trial. *JAMA Neurol*. 2022 Oct;79(10):1064-8. Available from: <https://doi.org/10.1001/jamaneurol.2022.2741>.
- [14] Harmsen IE, Wolff Fernandes F, Krauss JK, Lozano AM. Where Are We with Deep Brain Stimulation? A Review of Scientific Publications and Ongoing Research. *Stereotactic and Functional Neurosurgery*. 2022 02;100(3):184-97. Available from: <https://doi.org/10.1159/000521372>.
- [15] Hollunder B, Ostrem JL, Sahin IA, Rajamani N, Oxenford S, Butenko K, et al. Mapping dysfunctional circuits in the frontal cortex using deep brain stimulation. *Nature Neuroscience*. 2024 Mar;27(3):573-86. Available from: <https://doi.org/10.1038/s41593-024-01570-1>.
- [16] Neumann WJ, Gilron R, Little S, Tinkhauser G. Adaptive Deep Brain Stimulation: From Experimental Evidence Toward Practical Implementation. *Movement Disorders*. 2023;38(6):937-48. Available from: <https://movementdisorders.onlinelibrary.wiley.com/doi/abs/10.1002/mdr.24150>.
- [17] Lozano AM, Lipsman N, Bergman H, Brown P, Chabardes S, Chang JW, et al. Deep brain stimulation: current challenges and future directions. *Nat Rev Neurol*. 2019 Mar;15(3):148-60.
- [18] Hariz M, Blomstedt P. Deep brain stimulation for Parkinson's disease. *Journal of Internal Medicine*. 2022;292(5):764-78. Available from: <https://onlinelibrary.wiley.com/doi/abs/10.1111/jim.15441>.
- [19] Jakobs M, Fomenko A, Lozano AM, Kiening KL. Cellular, molecular, and clinical mechanisms of action of deep brain stimulation—a systematic review on established indications and outlook on future developments. *EMBO Molecular Medicine*. 2019;11(4):e9575. Available from: <https://www.embopress.org/doi/abs/10.15252/emmm.201809575>.
- [20] Hamani C, Temel Y. Deep brain stimulation for psychiatric disease: contributions and validity of animal models. *Sci Transl Med*. 2012 Jul;4(142):142rv8. Available from: <https://doi.org/10.1126/scitranslmed.3003722>.
- [21] Habets JGV, Heijmans M, Kuijf ML, Janssen MLF, Temel Y, Kubben PL. An update on adaptive deep brain stimulation in Parkinson's disease. *Movement Disorders*. 2018;33(12):1834-43. Available from: <https://movementdisorders.onlinelibrary.wiley.com/doi/abs/10.1002/mdr.1475>.
- [22] Little S, Pogosyan A, Neal S, Zavala B, Zrinzo L, Hariz M, et al. Adaptive deep brain stimulation in advanced Parkinson disease. *Annals of Neurology*. 2013;74(3):449-57. Available from: <http://dx.doi.org/10.1002/ana.23951>.
- [23] Arlotti M, Colombo M, Bonfanti A, Mandat T, Lanotte MM, Pirola E, et al. A New Implantable Closed-Loop Clinical Neural Interface: First Application in Parkinson's Disease. *Front Neurosci*. 2021 Dec;15:763235. Available from: <https://doi.org/10.3389/fnins.2021.763235>.
- [24] Swann NC, de Hemptinne C, Thompson MC, Miocinovic S, Miller AM, Gilron R, et al. Adaptive deep brain stimulation for Parkinson's disease using motor cortex sensing. *J Neural Eng*. 2018 May;15(4):046006. Available from: <https://doi.org/10.1088/1741-2552/aabc9b>.
- [25] Velisar A, Syrkin-Nikolau J, Blumenfeld Z, Trager MH, Afzal MF, Prabhakar V, et al. Dual threshold neural closed loop deep brain stimulation in Parkinson disease patients. *Brain Stimulation*. 2019;12(4):868-76. Available from: <https://doi.org/10.1016/j.brs.2019.04.001>.
- [26] Piña-Fuentes D, van Dijk JMC, van Zijl JC, Moes HR, van Laar T, Oterdoom DLM, et al. Acute effects of adaptive Deep Brain Stimulation in Parkinson's disease. *Brain Stimulation*. 2020;13(6):1507-16. Available from: <https://www.sciencedirect.com/science/article/pii/S1935860120300575>.
- [27] Scangos KW, Khambhati AN, Daly PM, Makhoul GS, Sugrue LP, Zamanian JH, et al. Closed-loop neuromodulation in an individual with treatment-resistant depression. *Nature Medicine*. 2021 Oct;27(10):1696-700. Available from: <https://doi.org/10.1038/s41591-021-01480-w>.
- [28] Gilron R, Little S, Wilt R, Perrone R, Anso J, Starr PA. Sleep-Aware Adaptive Deep Brain Stimulation Control: Chronic Use at Home With Dual Independent Linear Discriminate Detectors. *Frontiers in Neuroscience*. 2021;15. Available from: <https://www.frontiersin.org/journals/neuroscience/article/abs/10.3389/fnins.2021.675111>.

- tions Mgt. Unit; 2007. 08-038. Available from: <https://ssrn.com/abstract=1071720>.
- [44] Talmon JL, van Bommel JH. The advantage of modular software design in computerized ECG analysis. *Med Inform (Lond)*. 1986 Apr;11(2):117-28. Available from: <https://doi.org/10.3109/14639238609001365>.
- [45] Gastinger S, Hennicker R, Stabl R. In: Broy M, Jähnichen S, editors. Design of modular software systems with reuse. Berlin, Heidelberg: Springer Berlin Heidelberg; 1995. p. 112-27. Available from: <https://doi.org/10.1007/BFb0015458>.
- [46] Sullivan KJ, Griswold WG, Cai Y, Hallen B. The structure and value of modularity in software design. *SIGSOFT Softw Eng Notes*. 2001 sep;26(5):99-108. Available from: <https://doi.org/10.1145/503271.503224>.
- [47] Schalk G, McFarland DJ, Hinterberger T, Birbaumer N, Wolpaw JR. BCI2000: a general-purpose brain-computer interface (BCI) system. *IEEE Transactions on Biomedical Engineering*. 2004;51(6):1034-43.
- [48] Siegle JH, López AC, Patel YA, Abramov K, Ohayon S, Voigts J. Open Ephys: an open-source, plugin-based platform for multichannel electrophysiology. *Journal of Neural Engineering*. 2017 jun;14(4):045003. Available from: <https://dx.doi.org/10.1088/1741-2552/aa5eea>.
- [49] Renard Y, Lotte F, Gibert G, Congedo M, Maby E, Delannoy V, et al. OpenViBE: An Open-Source Software Platform to Design, Test, and Use Brain-Computer Interfaces in Real and Virtual Environments. *Presence: Teleoperators and Virtual Environments*. 2010 02;19(1):35-53. Available from: <https://doi.org/10.1162/pres.19.1.35>.
- [50] Ciliberti D, Kloosterman F. Falcon: a highly flexible open-source software for closed-loop neuroscience. *Journal of Neural Engineering*. 2017 jun;14(4):045004. Available from: <https://dx.doi.org/10.1088/1741-2552/aa7526>.
- [51] Ali YH, Bodkin K, Rigotti-Thompson M, Patel K, Card NS, Bhaduri B, et al. BRAND: a platform for closed-loop experiments with deep network models. *J Neural Eng*. 2024 Apr;21(2).
- [52] Clisson P, Bertrand-Lalo R, Congedo M, Victor-Thomas G, Chatel-Goldman J. Timeflux: an open-source framework for the acquisition and near real-time processing of signal streams. In: *BCI 2019 - 8th International Brain-Computer Interface Conference*. Graz, Austria; 2019. Available from: <https://hal.science/hal-02315098>.
- [53] Memmott T, Koçanaoğulları A, Lawhead M, Klee D, Dudy S, Fried-Oken M, et al. BciPy: brain-computer interface software in Python. *Brain-Computer Interfaces*. 2021;8(4):137-53. Available from: <https://doi.org/10.1080/2326263X.2021.1878727>.
- [54] Blankertz B, Acqualagna L, Dähne S, Haufe S, Schultze-Kraft M, Sturm I, et al. The Berlin Brain-Computer Interface: Progress Beyond Communication and Control. *Frontiers in Neuroscience*. 2016;10. Available from: <https://www.frontiersin.org/journals/neuroscience/article>
- [55] Venthur B, Scholler S, Williamson J, Dähne S, Treder MS, Kramarek MT, et al. Pyff—A Pythonic Framework for Feedback Applications and Stimulus Presentation in Neuroscience. *Frontiers in Neuroscience*. 2010;4. Available from: <https://www.frontiersin.org/journals/neuroscience/article>
- [56] Oostenveld R, Fries P, Maris E, Schoffelen JM. FieldTrip: Open Source Software for Advanced Analysis of MEG, EEG, and Invasive Electrophysiological Data. *Computational Intelligence and Neuroscience*. 2010 Dec;2011:156869. Available from: <https://doi.org/10.1155/2011/156869>.
- [57] Santamaría-Vázquez E, Martínez-Cagigal V, Marcos-Martínez D, Rodríguez-González V, Pérez-Velasco S, Moreno-Calderón S, et al. MEDUSA©: A novel Python-based software ecosystem to accelerate brain-computer interface and cognitive neuroscience research. *Computer Methods and Programs in Biomedicine*. 2023;230:107357. Available from: <https://www.sciencedirect.com/science/article/pii/S01692>
- [58] Kothe C, Shirazi SY, Stenner T, Medine D, Boulay C, Grivich MI, et al. The Lab Streaming Layer for Synchronized Multimodal Recording. *bioRxiv*. 2024. Available from: <https://www.biorxiv.org/content/early/2024/02/14/2024.02>
- [59] Kothe C, Medine D, Boulay C, Grivich M, Stenner T. LabStreamingLayer; 2024. GitHub repository. Available from: <https://github.com/sccn/labstreaminglayer>.
- [60] Fielding R, Nottingham M, Reschke J. RFC 9110: HTTP Semantics. USA: RFC Editor; 2022.
- [61] Ester M, Kriegel HP, Sander J, Xu X. A density-based algorithm for discovering clusters in large

- spatial databases with noise. In: Proceedings of the Second International Conference on Knowledge Discovery and Data Mining. AAAI Press; 1996. p. 226-31.
- [62] Ledoit O, Wolf M. A well-conditioned estimator for large-dimensional covariance matrices. *Journal of Multivariate Analysis*. 2004;88(2):365-411.
- [63] Bollinger J. *Bollinger on Bollinger Bands*. McGraw-Hill; 2002.
- [64] Thielen J, Marsman P, Farquhar J, Desain P. From full calibration to zero training for a code-modulated visual evoked potentials for brain-computer interface. *Journal of Neural Engineering*. 2021 apr;18(5):056007. Available from: <https://dx.doi.org/10.1088/1741-2552/abecef>.
- [65] Sutter EE. The brain response interface: communication through visually-induced electrical brain responses. *Journal of Microcomputer Applications*. 1992;15(1):31-45. Special Issue on Computers for Handicapped People. Available from: <https://www.sciencedirect.com/science/article/pii/S0145138990004571>.
- [66] Martínez-Cagigal V, Thielen J, Santamaría-Vázquez E, Pérez-Velasco S, Desain P, Hornero R. Brain-computer interfaces based on code-modulated visual evoked potentials (c-VEP): a literature review. *Journal of Neural Engineering*. 2021 nov;18(6):061002. Available from: <https://dx.doi.org/10.1088/1741-2552/ac38cf>.
- [67] Thielen J, van den Broek P, Farquhar J, Desain P. Broad-Band Visually Evoked Potentials: Re(con)volution in Brain-Computer Interfacing. *PLOS ONE*. 2015 07;10(7):1-22. Available from: <https://doi.org/10.1371/journal.pone.0133797>.
- [68] Dold M, Pereira J, Thielen J, Sajonz B, Coenen VA, Tangermann M. Dareplane data for proof of concept paper. Radboud University; 2024. Available from: <https://doi.org/10.34973/d214-m34>.
- [69] Artoni F, Barsotti A, Guanziroli E, Micera S, Landi A, Molteni F. Effective Synchronization of EEG and EMG for Mobile Brain/Body Imaging in Clinical Settings. *Frontiers in Human Neuroscience*. 2018;11. Available from: <https://www.frontiersin.org/articles/10.3389/fnhum.2017.00652>.
- [70] Schulte RV, Prinsen EC, Schaake L, Buurke JH. Synchronization of wearable motion capture and EMG measurement systems. *IEEE Int Conf Rehabil Robot*. 2022 Jul;2022:1-6.
- [71] Chuang CH, Lu SW, Chao YP, Peng PH, Hsu HC, Hung CC, et al. Near-zero phase-lag hyperscanning in a novel wireless EEG system. *Journal of Neural Engineering*. 2021 nov;18(6):066010. Available from: <https://dx.doi.org/10.1088/1741-2552/ac33e6>.
- [72] Martin RC. *Design Principles and Design Patterns*; 2000. Accessed: 2024-05-22. https://staff.cs.utu.fi/~jounsmmed/doos_06/material/Design
- [73] Appelhoff S, Stenner T. In COM we trust: Feasibility of USB-based event marking. *Behav Res Methods*. 2021 Apr;53(6):2450-5. Available from: <https://doi.org/10.3758/s13428-021-01571-z>.
- [74] Tinkhauser G, Pogosyan A, Little S, Beudel M, Herz DM, Tan H, et al. The modulatory effect of adaptive deep brain stimulation on beta bursts in Parkinson's disease. *Brain*. 2017 02;140(4):1053-67. Available from: <https://doi.org/10.1093/brain/awx010>.
- [75] Patel YA, George A, Dorval AD, White JA, Christini DJ, Butera RJ. Hard real-time closed-loop control of the Real-Time eXperiment Interface (RTXI). *PLOS Computational Biology*. 2017 05;13(5):1-22. Available from: <https://doi.org/10.1371/journal.pcbi.1005430>.
- [76] Gilron R, Little S, Perrone R, Wilt R, de Hemptinne C, Yaroshinsky MS, et al. Long-term wireless streaming of neural recordings for circuit discovery and adaptive stimulation in individuals with Parkinson's disease. *Nature Biotechnology*. 2021 Sep;39(9):1078-85. Available from: <https://doi.org/10.1038/s41587-021-00897-5>.
- [77] Rosa M, Arlotti M, Ardolino G, Cogiamanian F, Marceglia S, Di Fonzo A, et al. Adaptive deep brain stimulation in a freely moving parkinsonian patient. *Movement Disorders*. 2015;30(7):1003-5. Available from: <http://dx.doi.org/10.1002/mds.26241>.
- [78] Abdi-Sargezeh B, Shirani S, Sharma A, Green A, Akram H, Zrinzo L, et al. Prediction of pathological subthalamic nucleus beta burst occurrence in Parkinson's disease. *bioRxiv*. 2024. Available from: <https://www.biorxiv.org/content/early/2024/05/10/2024.05.10.591204>.
- [79] Pogosyan A, Tan H, Herz DM, Kühn AA, Brown P. Beta burst dynamics in Parkinson's disease OFF and ON dopaminergic medication. *Brain*.

- 2017 10;140(11):2968-81. Available from: <https://doi.org/10.1093/brain/awx252>.
- [80] Holt AB, Kormann E, Gulberti A, Pötter-Nerger M, McNamara CG, Cagnan H, et al. Phase-Dependent Suppression of Beta Oscillations in Parkinson's Disease Patients. *Journal of Neuroscience*. 2019;39(6):1119-34. Available from: <https://www.jneurosci.org/content/39/6/1119>.
- [81] Cagnan H, Pedrosa D, Little S, Pogosyan A, Cheeran B, Aziz T, et al. Stimulating at the right time: phase-specific deep brain stimulation. *Brain*. 2016 12;140(1):132-45. Available from: <https://doi.org/10.1093/brain/aww286>.
- [82] McNamara CG, Rothwell M, Sharott A. Stable, interactive modulation of neuronal oscillations produced through brain-machine equilibrium. *Cell Reports*. 2022;41(6):111616. Available from: <https://www.sciencedirect.com/science/article/pii/S2211124722014851>.
- [83] West TO, Magill PJ, Sharott A, Litvak V, Farmer SF, Cagnan H. Stimulating at the right time to recover network states in a model of the cortico-basal ganglia-thalamic circuit. *PLOS Computational Biology*. 2022 03;18(3):1-32. Available from: <https://doi.org/10.1371/journal.pcbi.1009887>.
- [84] Iwama S, Takemi M, Eguchi R, Hirose R, Morishige M, Ushiba J. Two common issues in synchronized multimodal recordings with EEG: Jitter and latency. *Neuroscience Research*. 2023. Available from: <https://www.sciencedirect.com/science/article/pii/S0168010223002201>.
- [85] Haufe S, Meinecke F, Görden K, Dähne S, Haynes JD, Blankertz B, et al. On the interpretation of weight vectors of linear models in multivariate neuroimaging. *NeuroImage*. 2014;87:96-110. Available from: <https://www.sciencedirect.com/science/article/pii/S1053811913010914>.
- [86] Dasenbrock S, Blum S, Maanen P, Debener S, Hohmann V, Kayser H. Synchronization of ear-EEG and audio streams in portable research hearing device. *Front Neurosci*. 2022 Sep;16:904003.